LLE Review
Quarterly Report

UR
LLE

LLE Review

Quarterly Report

April, 1981 — June, 1981

UR
LLE

IN BRIEF

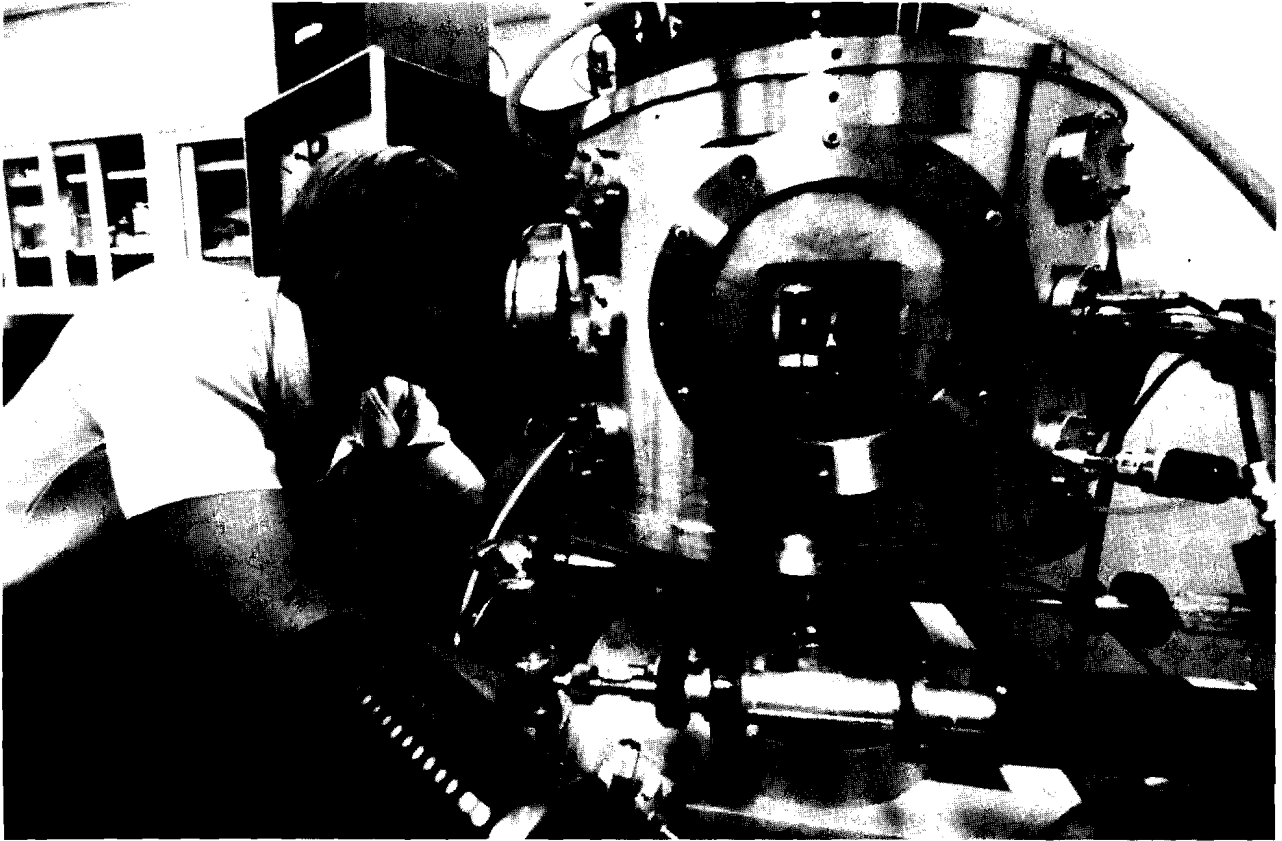In this quarter there have been several exciting developments at LLE:

- The first implosion experiments on the OMEGA facility yielded in excess of 10^{10} neutrons per shot using "exploding pusher" DT-filled microballoons.

- Detailed measurements of backscattered spectra have been made on the tripled frequency GDL glass laser system observing both Brillouin and Raman scattered light. Thresholds were observed as was saturation at rather low levels.

- Two NLUF users are conducting experiments at LLE, a third will begin next quarter. Six new proposals have been approved by the NLUF Steering Committee for future experiments.

- Our facility for damage testing optical coatings is now on-line. A variety of AR and HR coatings have been tested at 0.351 μm with measured damage thresholds between 0.5 and 2.5 J/cm².

- The Research Advisory Board met at LLE on May 6, 1981 to review the Laboratory's program. Their preliminary statement strongly endorsed our plans to convert the OMEGA laser system to the UV (0.351 μm).

CONTENTS

Jerry Drumheller operates the target fabrication group's ion beam sputtering system. This is the first use of this device for depositing high-Z fusion target pusher layers. The results of a series of experiments using this method are reported in this issue.

Section 1
LASER SYSTEM REPORT

1.A GDL Facility Report

During the third quarter of FY 81, GDL continued operations as a 0.35 μm irradiation facility

A total of 690 shots were delivered by the facility in the April 1 to June 30, 1981 period. The shot distribution was as follows:

3ω target experiments	53 Shots
x-ray program	60
damage test facility	560
alignment	17
	total 690 Shots

The results of the 3ω interaction experiments continued to support previous expectations of improved overall coupling efficiency with 0.35 μm compared to 1 μm radiation. In the last series of experiments ablation pressure, mass ablation rate and preliminary preheat measurements have been conducted. The ablation pressure was found to increase nearly linearly with irradiance and was 70 Mbar at 10^{15} W/cm². Preheat as evidenced by Kα x-ray line emission is significantly lower than in 1.05 μm irradiation. Measurements have also been made of the threshold, gain and saturation of the stimulated Raman scattering instability that we discussed elsewhere in this report.

During this quarter a significant amount of work was conducted on the damage testing facility. Promising index matching liquids

for 0.35 μm operations were identified and tested successfully. In addition a variety of anti-reflection and high reflectance coatings for 0.35 μm operation were tested. Some of these coatings performed well enough to be considered for use in the planned conversion of OMEGA to an ultraviolet irradiation facility.

1.B Laser Damage Testing of Optical Coatings at 351 nm

As the laser fusion community begins to frequency convert their Nd:glass lasers to shorter wavelengths, the importance of the performance of optical coatings at these wavelengths becomes of great interest. Of particular interest at LLE is the performance of these coatings at the tripled frequency of Nd:glass, 351 nm. The level at which the optical coatings can transport the UV beam will have a major impact on the size, cost and energy on target in any UV upgrade of OMEGA.

Over the last several years a major effort has gone into measuring and attempting to improve the damage thresholds of optical coatings at 1.06 μm[1]. There has been very little done at shorter wavelengths[2,3]. What has been done has shown that damage thresholds are considerably lower than those at 1.06 μm. State-of-the-art coatings for 1.06 μm have damage thresholds for 1 ns pulses of 6 to 10 J/cm^2 for high reflectors (HR) and 4 to 7 J/cm^2 for anti-reflectors (AR).[1] Our measured damage thresholds for 351 nm light in 400 psec pulses have been found to be 0.5 to 2.5 J/cm^2 for HR coatings and 2.5 J/cm^2 for an AR coating.

A diagram of the apparatus used to measure the damage thresholds is shown in Fig. 1. Damage testing is done by irradiating a given sample and characterizing the incident light pulses' energy, spatial intensity distribution and pulse width. These parameters change from shot to shot, so it is imperative that they be accurately determined. After irradiating the sample one must decide which laser pulses actually caused damage.

The LLE UV damage tester uses the output of the Glass Development Laser (GDL) after the 40 mm rod amplifier. Firing through the 40 mm amplifier gives typically an output of 1.6 J of 1.06 μ light and the laser system can be fired every 10 minutes. This output is directed to a set of KDP crystals operated in a similar manner to Seka, et al.[4] to produce 351 nm light. The efficiency of conversion is 60%. The residual 1.06 μm and 0.53 μm light from the tripling process is removed by a dichroic mirror and the 0.35 μm light is then focused down onto the coating sample. A half wave plate and a set of two dielectric polarizers are used to throttle the amount of energy that is delivered onto the sample. This keeps the loading on the KDP crystals the same for all intensities on the sample and as a result, keeps the beam profile and pulse width relatively constant during the tests. The beam is 5 mm in diameter when it strikes the sample.
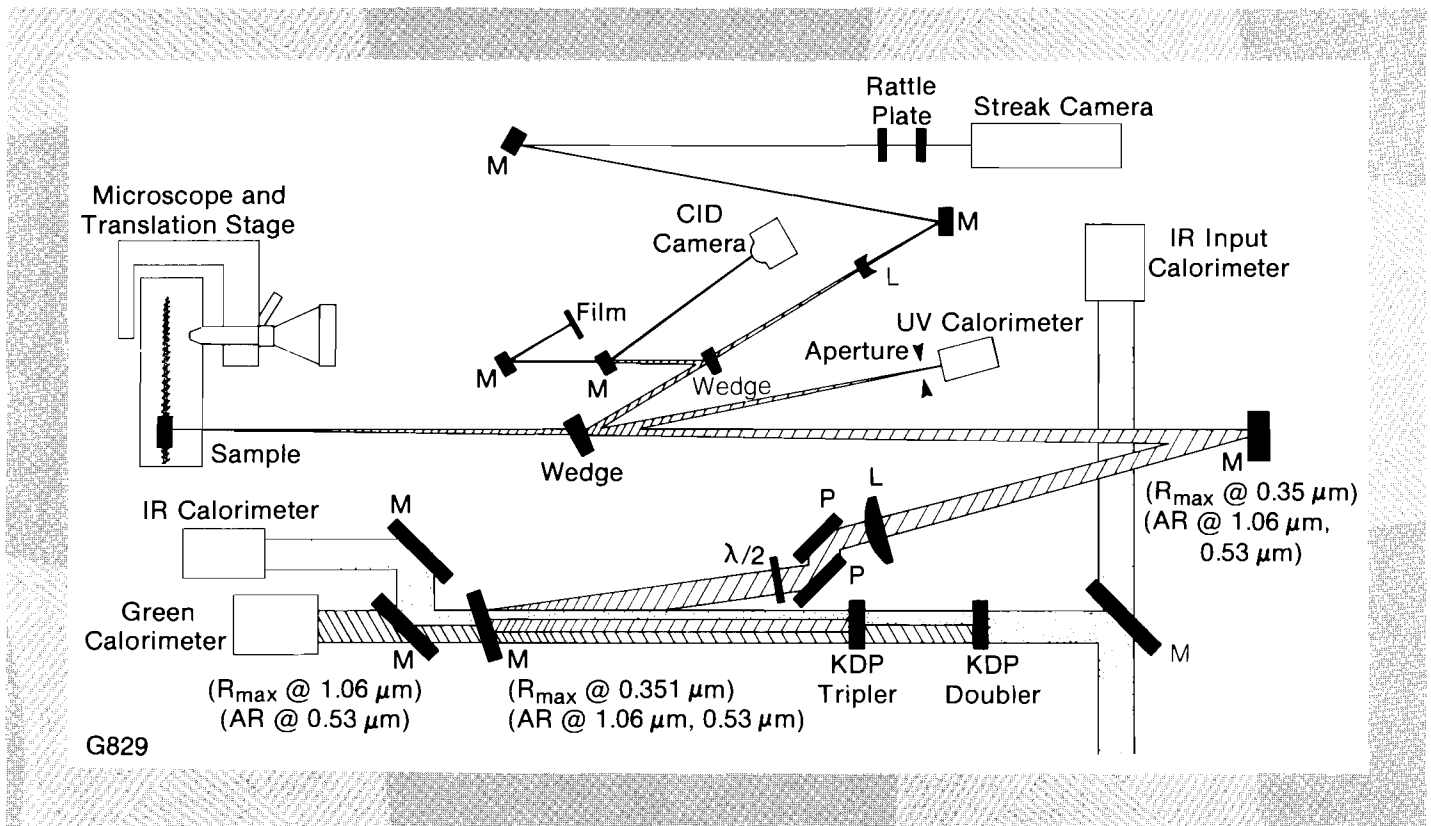
Fig. 1
0.35 μm damage tester.

An uncoated wedge picks off a portion of the beam and directs it to a set of diagnostics to measure the energy, pulse width and intensity profile of the beam for each shot. The intensity profile is recorded both on film and a solid state TV camera. The TV image is recorded in a mini-computer with the aid of a high speed video digitizer. Figure 2 shows a block diagram of data collection system. The maximum energy density is determined from this spatial distribution and the total energy on the sample. This analysis takes approximately 8 minutes. The determination of damage is done by taking photo-micrographs of the portion of the sample that is irradiated, both before and after the shot.

Approximately 30 samples have been tested to date. The average results of these tests are summarized in Figs. 3 and 4. All but those noted of these samples were produced by University of Rochester coating shop. The preliminary results indicate that for 400 psec pulses damage thresholds for dielectric coatings with 351 μm light run from 0.5 to 3 J/cm². It is also interesting that AR coatings have a slightly higher threshold than the HR coatings. This is just the opposite of the results found for coatings at 1.06 μm. This probably indicates that we are seeing a bulk coating materials effect rather that usual interface problem.

The highest damage threshold that we have measured has been on AR treatment to BK-10 glass developed by Schott Glass. In this process, known as the "Schroeder Process," the surface of the glass is etched to a quarter wave depth by an acid, leaving the

3

Data

Calorimeter

Video

Trigger

A to D

LeCroy
Digitizer

Buffer

Camac

Chromatics
Computer

HP-2100S
Computer

Color
Monitor

TTY
Graphics

Disk

G827
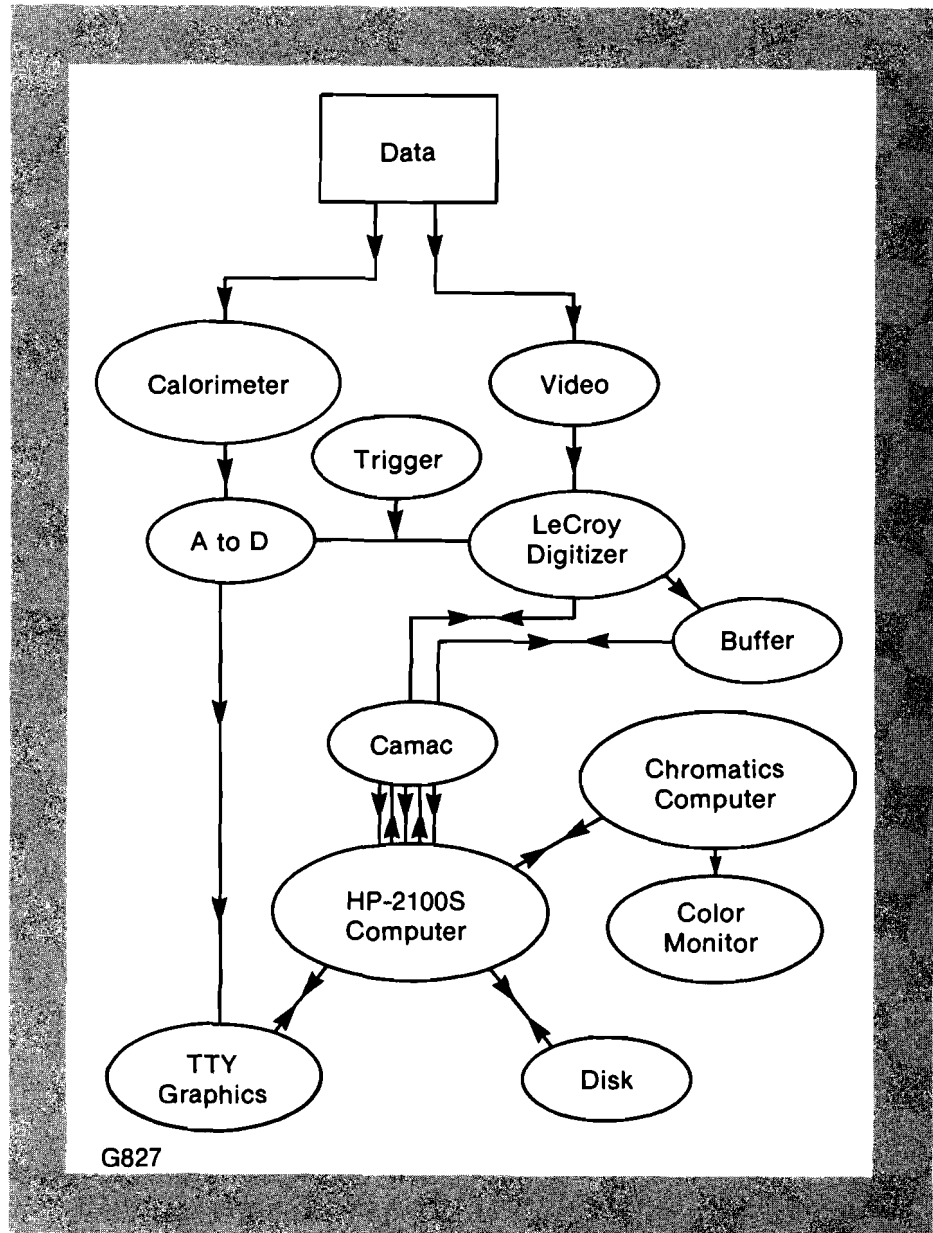
Fig. 2
Image analysis hardware.

surface with a reflectivity less than 0.5%. Previous surface treatments[5] to produce AR properties have not been very durable and could not be cleaned. The Schroeder process is cleanable and appears fairly durable. This, plus a damage threshold of 9 J/cm^2 makes this coating look very promising for future UV systems.

This initial set of data gives the laser designers a good idea of the state-of-the-art of UV coatings. In the next several months a series of tests on additional coatings will be performed as the coatings engineers begin to vary materials and deposition parameters in an attempt to improve damage thresholds at 351 nm.

Materials	Threshold (J/cm^2)
	$\pm 0.2\ J/cm^2$
•Y_2O_3 (AR @ 0.35 μm)	2.5 [4 samples]
• Schott Schroeder Process	9.0 [2 samples]

G823

Fig. 3
Damage thresholds of AR coatings.

Material	Threshold (J/cm^2)
	$\pm 0.2\ J/cm^2$
• Ta_2O_5 (HR @ 45°)	1.8 [8 samples]
• Ta_2O_5 (HR @ 0°, AR for 1.06 μ, 0.53μ)	1.7 [1 sample]
• HfO_2* (HR @ 0°)	0.75 [1 sample]
• ZrO_2*	1.8 [1 sample]
• Ta_2O_5* (HR @ 0°)	1.7 [1 sample]

*supplied by D. Milam, LLNL
G824

Fig. 4
Damage thresholds of HR coatings.

REFERENCES

1. *Optical Coatings – Applications and Utilization II, SPIE* vol. **140** (1978).

2. T. F. Douton and W. L. Smith, *1979 Symposium on Materials for High Power Lasers, NBS Special Publication* **568** (1979).

3. B. E. Newman and D. H. Gill, *1978 Symposium on Materials for High Power Lasers, NBS Special Publication* **541** (1978).

4. W. Seka, S. D. Jacobs, J. E. Rizzo, R. Boni, and S. Craxton, *Opt. Comm.* **34**, 469 (1980).

3. M. J. Monot, *J. Opt. Soc. Am.* **66**, 515 (1976).

1.C Beam Uniformity Measurements on the OMEGA Laser

The OMEGA laser facility utilizes 24 beams to uniformly illuminate a spherical target. To achieve uniform compression theoretical predictions indicate that the uniformity of the intensity in each beam must be within 5-10%.[1] Measurements have been made of the intensity distribution, phase profile and far field intensity

distribution of a single beam of the laser system. We have used a computer code (Beamprop) to simulate the intensity patterns on target using the amplitude and phase measurements on the beam at the input to the OMEGA focus lens. Using this code, we have investigated the effects of spherical aberration upon the intensity at the target plane.

Measurements of the OMEGA beam have been made at long pulse (600 psec) and short pulse (100 psec). Beam diagnostic packages were modified to take pictures of the phase profile of the beam and the equivalent target plane intensity both at the end of the laser and at the plane of the OMEGA focus lens, a propagation distance of approximately 20 meters.[2] These data support the initial conclusion[1] that this propagation distance does not affect the laser intensity on target.

The phase profile was measured using a double frequency lateral shear interferometer. Figure 5 shows two orthogonal shear photos of a single shot. Fringes which show departure from a straight line indicate aberration, and these shear patterns show the laser beam phase departs from a perfect plane wave front. The wave front aberrations are not rotationally symmetric, but a single average between the horizontal and the vertical cross sections indicate that there is need for spherical correction of the wave front. The shear pattern photographs were evaluated by measuring the fringe locations on a diagonal along the shear direction. These positions and their corresponding order numbers
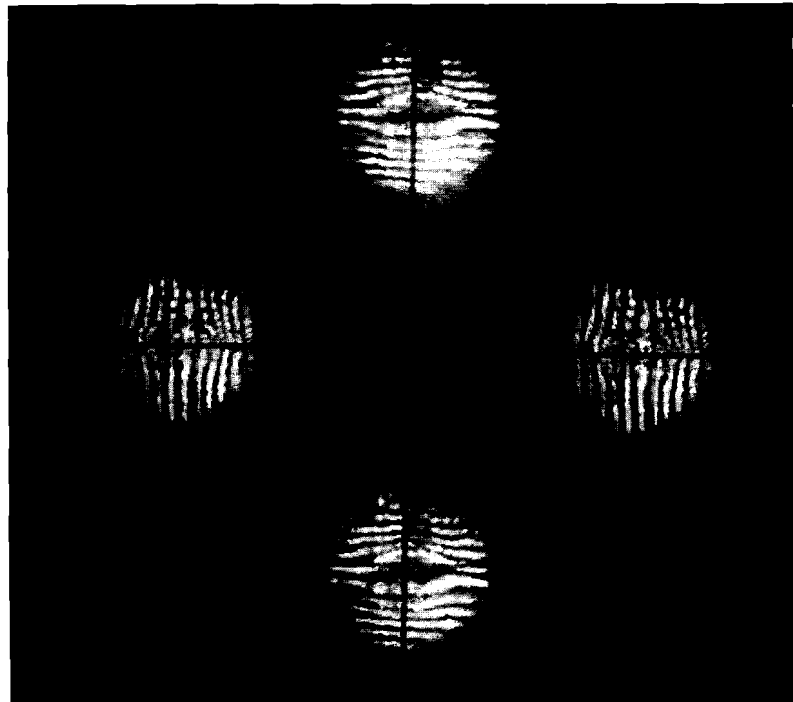

Fig. 5
Shot #5594 (beam power 340 GW, 100 psec pulse.)

were then inserted into a program that computed the wave front aberration polynomial assuming the data represented a rotationally symmetrical wave front. The same procedure was then repeated for the orthogonal shear. In this way, two cross sections of the wave front were found. Table 1 lists some of the resulting computed wave fronts for 100 psec pulses.

SHOT #	POWER	HORIZONTAL SCAN				VERTICAL SCAN			
		OPD2	OPD4	OPD6	OPD8	OPD2	OPD4	OPD6	OPD8
5596	316 GW	-3.37	-24.71	26.32	-9.21	-8.41	-8.46	5.56	-0.115
5595	240 GW	-8.06	-8.21	2.98	1.75	-6.19	-29.84	47.20	-22.80
5593	347 GW	-3.25	-31.26	44.70	-22.80	-4.65	-13.90	3.85	5.530
5591	260 GW	-7.72	-11.11	10.86	-3.80	-9.376	-4.91	-4.32	7.020

Table 1
The wave front coefficients as measured from the shearing photographs and fitted to an even eighth order polynomial.

Near field data was obtained by propagating the beam undisturbed onto a piece of film. These measurements were also made at the end of the laser and in the target bay to show any effects due to long path propagation. A typical photo is shown in Fig. 6.

Fig. 6
"Near field" photograph of laser beam at input to OMEGA focus lens (short pulse): shot #5596.

The far field image photographs were measured on a micro-densitometer and the data was processed in an image analysis program. Figure 7 shows a radially averaged plot of intensity from a 100 psec pulse at 1400 μm from best focus of the OMEGA lens. This 1400 μm corresponds to a focus shift of six target radii from best focus for a 400 μm diameter target. This focal shift has been predicted to give optimum uniformity on target.[1] Additional analysis of these photographic data is ongoing.
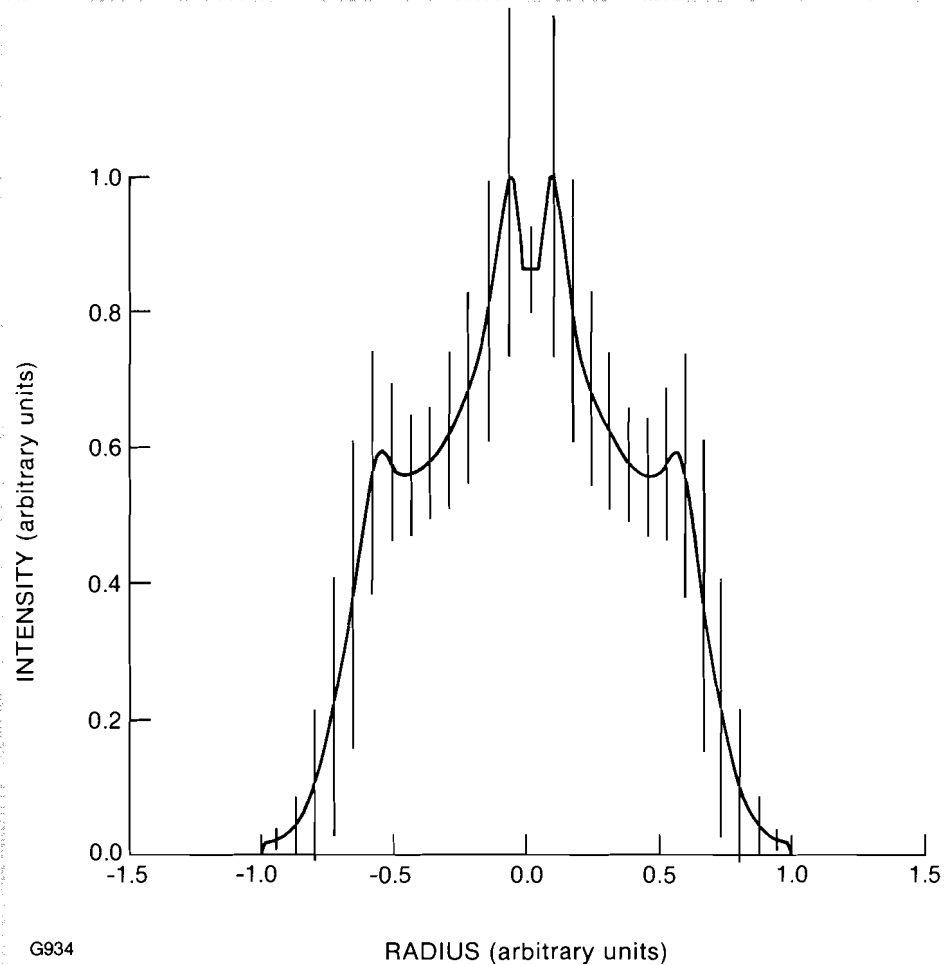
Fig. 7
Beam intensity 1400 μ from best focus
(radial average): shot #5596.

Beamprop is a Fast Fourier Transform diffraction code for the propagation of wave fronts through a homogeneous medium. With this program, it is possible to start with a spherical wave front and propagate it through a lens to an out of focus image plane which corresponds to the surface tangent to the target. It provides the intensity distribution of the image in that plane.

The program will accept phase profiles of an eighth order polynomial of spherical aberration assuming radial symmetry. Using this program the measured values of beam phase aberration can be inserted to compute the intensity distributions in the out of focus image plane. Figure 8 shows the distribution of intensity across the aperture of the focusing lens that was used to calculate the following far field intensity patterns. The focus lens was run at f/3.5 with a 60 cm focal length. Figure 9 is a plot of the far field pattern simulation 1400 μm from best focus when the wave front has zero aberration. Figure 10 shows the computed intensity distribution with phase aberration. The coefficients of the spherical aberration polynomial are shown on the figure. The
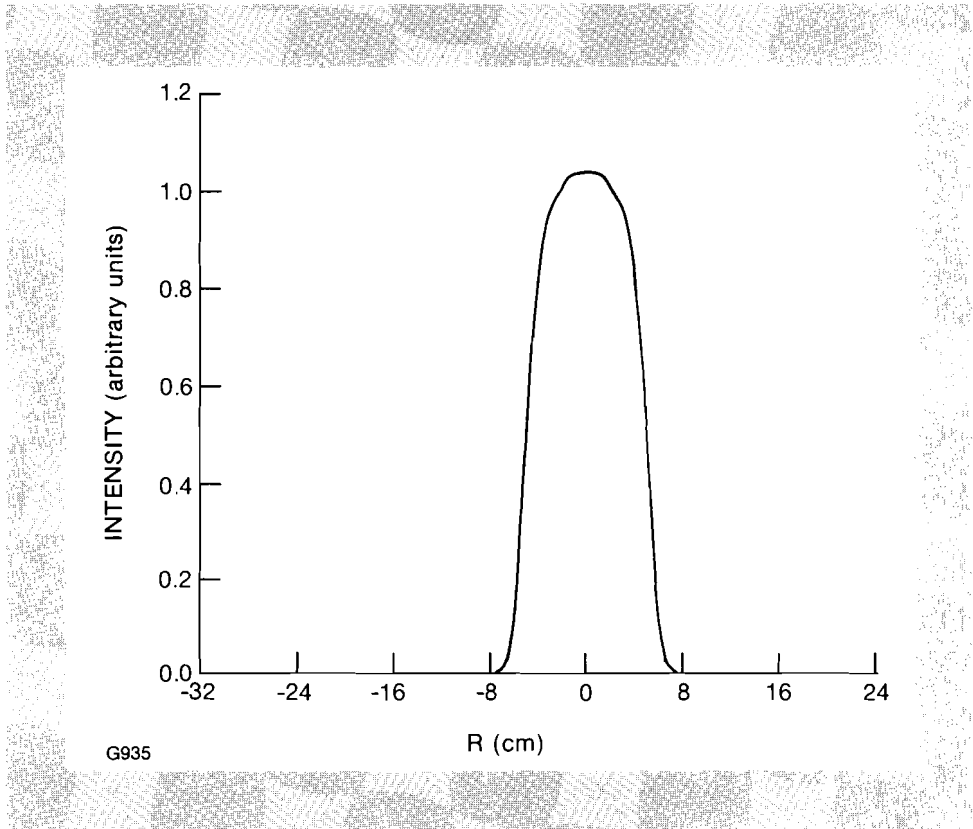
Fig. 8
Beam intensity distribution into OMEGA
f/3.4 lens (simulation).

intensity is peaked in the center in a fashion comparable to the real data of Fig. 8.
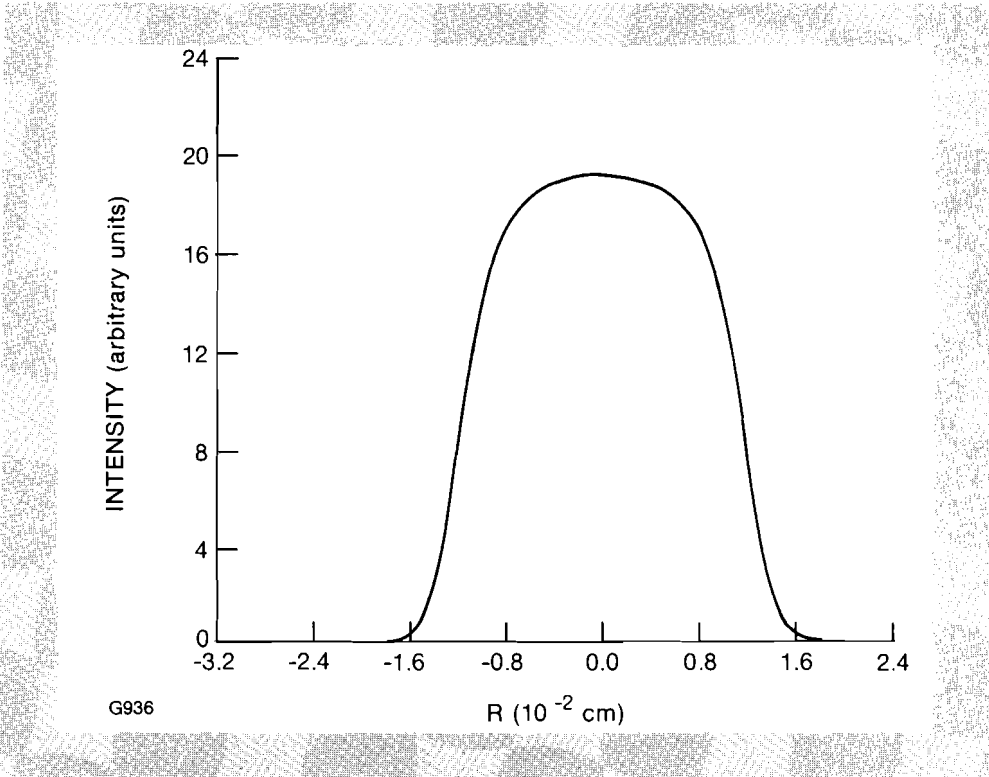

Fig. 9
Intensity pattern 1400 μ from best focus, no beam aberrations (simulation).
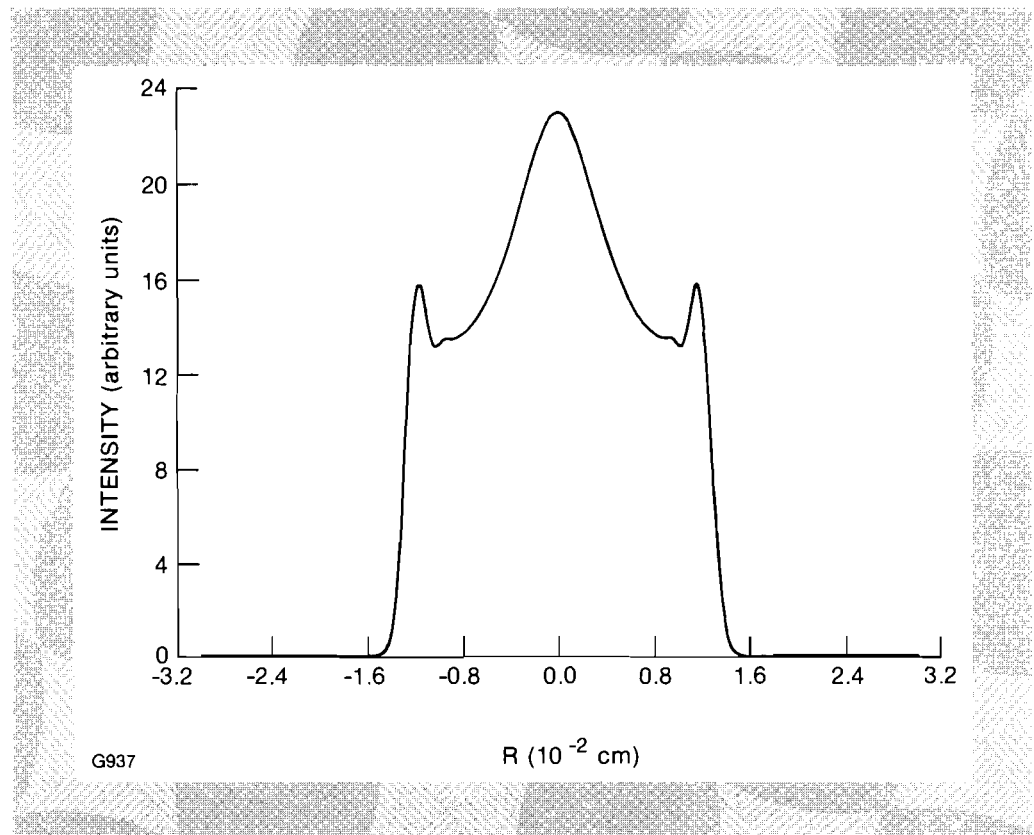
9

Fig. 10
Beam intensity 1400 μ from best focus
(simulation). Beam aberrations:
 − 13.6 waves third order
 + 28.3 waves fifth order
 − 15.0 waves seventh order
 + 1.3 waves focus

Two runs have been made using Beamprop to show the effects of pure positive and negative third order spherical aberration. These were run in order to illustrate a possible method of significantly modifying the intensity profile on target by the use of phase correction plates. The results are shown in Figs. 11 and 12. Positive third order optical path difference (OPD) (a leading wave front at the edge of the aperture) causes an inverse quadratic type of intensity distribution, as seen in Fig. 11, and negative OPD (a lagging wave front at the edge of the aperture) causes spreading of the image at the edge and a concentration in the center of the image, as seen in Fig. 12.

The performance of OMEGA at longer pulse length (~ 1 nsec) will be measured in the future. The correction of system phase aberration with fixed corrector plates or deformable mirrors will be evaluated. In addition, off line component testing will be utilized to understand the source of the phase aberrations.

REFERENCES

1. LLE Review vol. 4.

2. S. Kumpan, OMEGA Single Beam Characterization Preliminary Report, LLE Internal Report (1981).
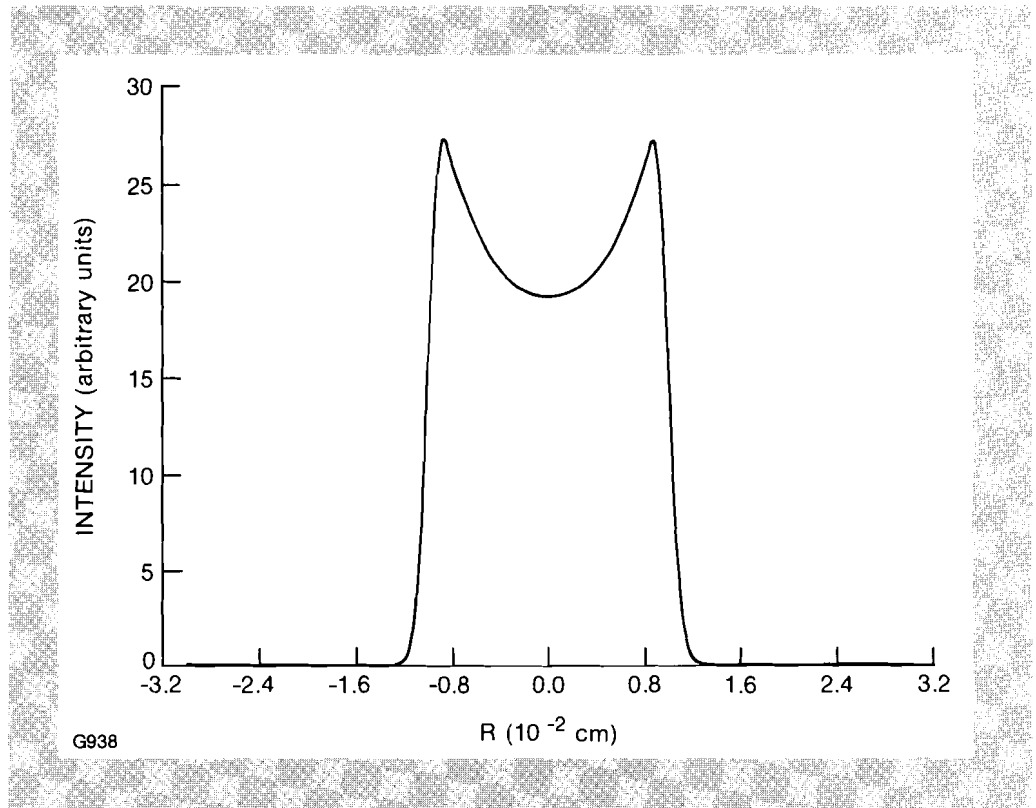
Fig. 11
Intensity pattern 1400 μ from best
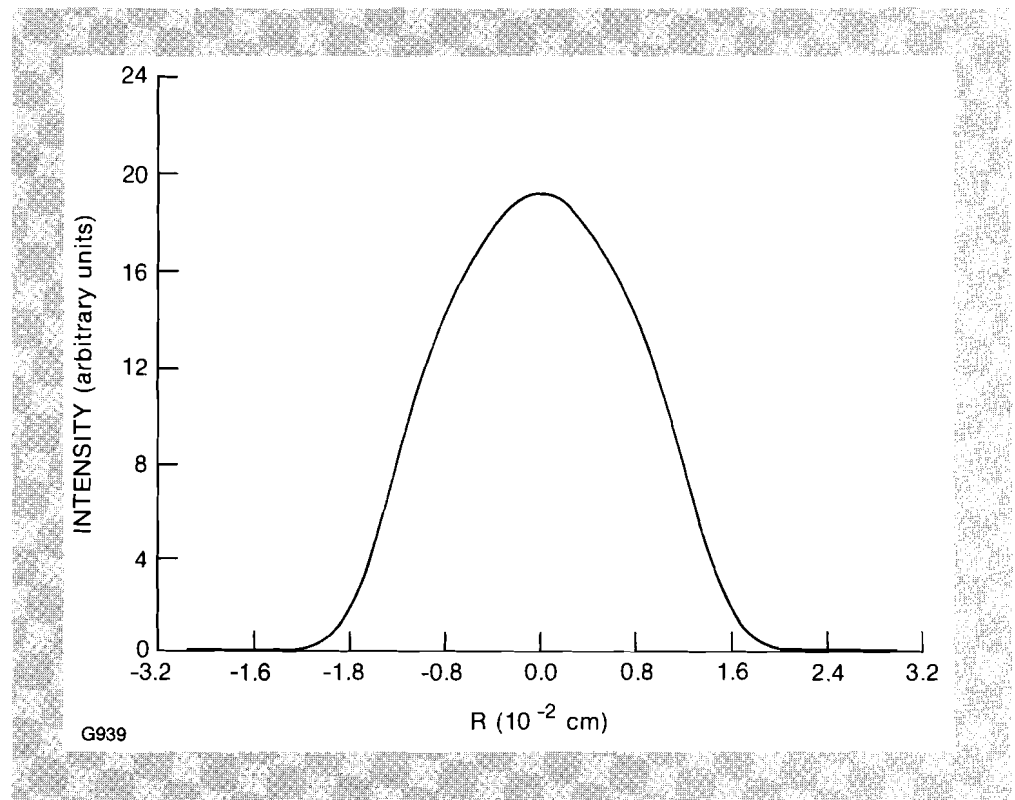focus (simulation). Beam aberrations:
  + 3 waves third order

Fig. 12
Intensity pattern 1400 μ
from best focus (simulation).
Beam aberrations:
    — 3 waves third order.

Section 2

PROGRESS IN LASER FUSION

2.A Initial Experiments on OMEGA

The OMEGA laser facility, a 24-beam neodymium phosphate glass system capable of peak output powers of the order of 12 TW at 75 psec duration pulses, and maximum output energies of the order of 4.8 KJ has recently become operational as a target irradiation facility. Six beams of this system have previously been utilized as the ZETA facility for an extensive series of short pulse (of the order of 75 psec) experiments at high intensities ($10^{15}-10^{17}$ W/cm^2) examining the behavior of thin and thick shell targets in what has become known as the "exploding pusher" regime, with symmetric irradiation.

In April of this year, 24-beam target experiments commenced on the OMEGA facility. This series of shots is also being run in the short pulse exploding pusher regime in order that the laser system performance and primary baseline diagnostics can be characterized under known operating conditions. Apart from this overall objective, the series of shots has three specific objectives:

1. To fully characterize the degree to which all 24-beams of OMEGA can routinely be positioned and targeted with high temporal and spatial accuracy, and to increase the confidence level in our ability to take a large number (up to 8) shots on each day that target experiments are scheduled.

2. To perform a selected series of 24-beam high power experiments with simple thin shell exploding pusher

targets, in a parametric region already well explored, to ensure full operation of primary experimental diagnostics such as plasma calorimetry, x-ray photography, and neutron diagnostics. In addition, these experiments permit the examination of scaling laws for symmetrically driven exploding pusher targets at higher powers than previously used at LLE.

3. To make an initial evaluation of the degree to which the uniformity of irradiation is a factor in the performance of these types of targets.

Although these experiments are still in progress, and thus the analysis of results tentative, several noteworthy achievements have been attained.

Tests specifically designed to determine beam pointing and focusing and target centering accuracy were made through x-ray photography of gold-coated spherical targets irradiated with symmetric six-beam combinations, each beam focused on the surface of the target. Examination of the sizes and relative positions of the individual x-ray images on the surface of the target then permitted estimation of the position of best focus for each beam and the beam pointing and centering accuracy. The axial position of focus could be estimated to an accuracy of the order of 50 μm, while it was found that individual beams could be routinely pointed with an accuracy of the order of 11 μm. This degree of accuracy in fact approaches the limits set by visualization and stability of the target. The maximum excursion of any individual beam recorded during these tests was of the order of 25 μm. In addition, the individual beamlines have been timed relative to one another to within 3 psec with the use of a CW laser interference technique.

A number of shots have been taken to examine scaling laws for exploding pusher targets irradiated by 24 beams with total on-target power levels of up to 8 TW and pulse durations of ~ 100 psec. Simple glass microballoon targets, filled with 20 atm of DT having diameters in the 150-250 μm range have been used and among other features the effects on target performance of variations in the imposed intensity distribution on target have been examined. In general, it was found that the overall laser light absorption is a strong function of beam focus position reaching a peak value of the order of 40% for center-focused beams. Neutron yield is found to scale with specific absorbed energy up to values of ~ 1 J/ngm, and in a series of six shots on May 19, three consecutive shots recorded yields in excess of 10^{10} neutrons at incident power levels of < 7 TW. The peak neutron yield so far obtained is 1.35×10^{10} neutrons. These results represent a considerable improvement in the overall yield efficiency so far attained in any laser fusion experiment (Fig. 13), yield efficiency being here defined as the ratio of the total energy in thermonuclear products to the total absorbed laser energy. In addition to the diagnostics quoted above, x-ray crystal spectrographic, neutron TOF, and x-ray micrographic measurements are
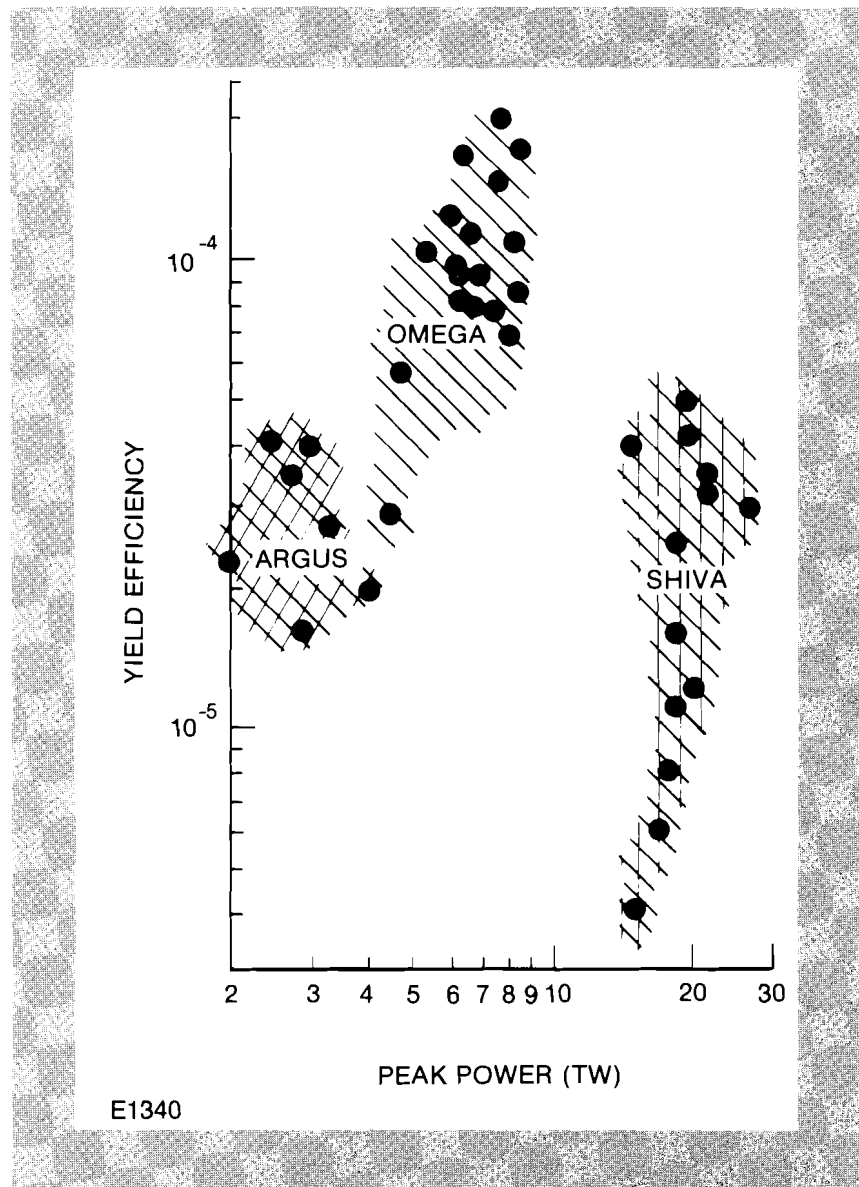
Fig. 13
Yield efficiency of exploding-pusher
targets.

being made as well as development of the so-called "knock-on" determination of fuel ρR through analysis of the spectra of elastically scattered deuterons and tritons. These investigations will be described in more detail in a later LLE Review when an overall summary of exploding pusher target experiments on OMEGA will be given.

2.B Stimulated Backscatter Measurements in the Laser Matter Interaction Experiments

Stimulated scattering processes of the incident laser light in the underdense plasma are potentially important in laser fusion. We have made observations of spectrally resolved backscatter light from simple planar targets illuminated with the 0.35 μm beam of the GDL laser (< 50 J at 400 psec). The measurements have included time and spectrally resolved measurements close to the incident wavelength to look for evidence of Brillouin scattering. Time integrated measurements in the spectral region between 0.40 and 0.70 μm were made to investigate Raman and two plasmon decay processes.

Under the condition of these experiments (3×10^{13} to 3×10^{15} W/cm^2 at 400 psec, and CH, Ni, or Au targets) we observe both Brillouin and Raman backscatter; the level of backscatter, however, is low (< 10^{-2} for SBS, < 10^{-6} for SRS).

The impact of these effects on future laser fusion experiments are quite different. Brillouin scattering is a process in which the incident electromagnetic (EM) wave is converted to an ion acoustic plasma wave and a scattered EM wave. Since the frequency of the ion acoustic wave is small compared to the EM wave, very little energy is delivered to the plasma by this process. This scattering mechanism is significant principally as an energy loss mechanism which might limit the coupling efficiency of the light to the plasma. In Fig. 14 we show the fraction of the energy

Fig. 14
*Percent backreflection versus laser intensity.*

E1288
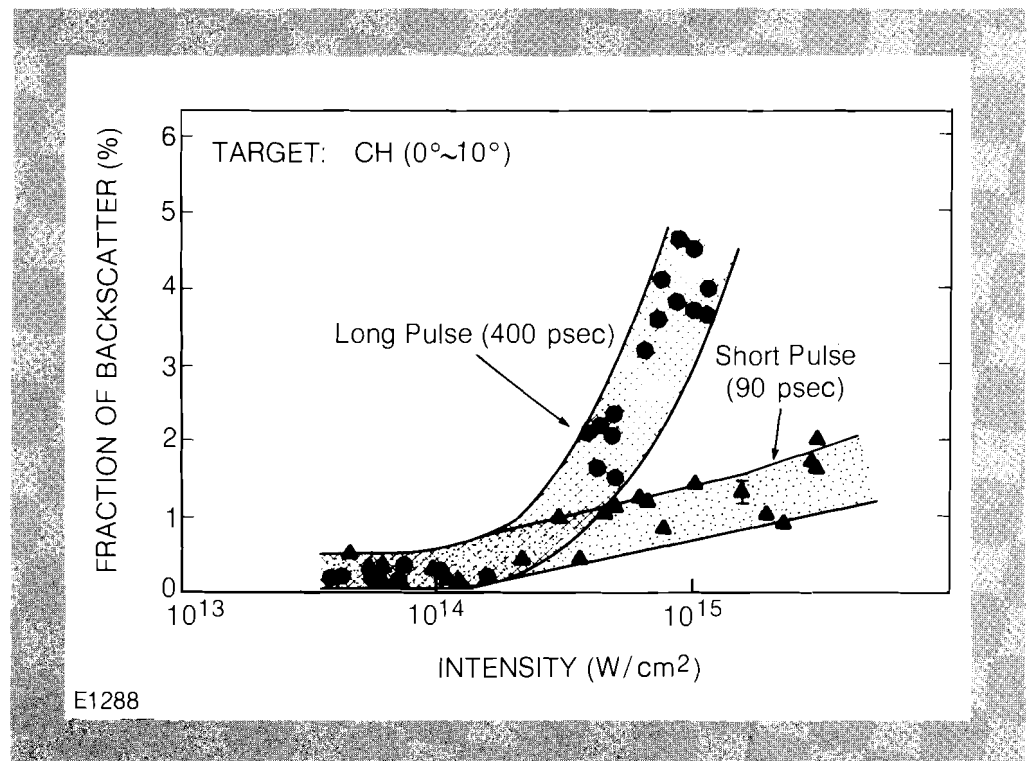
that was backscattered through the focusing lens (f/12) by Brillouin-type processes in these experiments. Even at the highest intensities these processes only led to a backscatter fraction of less than 5% of the incident light. However, due to our particular experimental set-up (f/12 focusing lens) we estimate that the real backscatter fraction may be up to twice the measured fraction.

A typical set of time-resolved observations is shown in Fig. 15. This figure shows iso-intensity contours of the backscattered light. In this figure, wavelength dispersion is shown in the vertical direction and time dispersion in the horizontal direction. The three cases are chosen to illustrate the qualitative change in the spectra observed for targets oriented at various angles with respect to the incident beam. The mean value of the spectral shift for the 22° targets is a 1 to 2 Å red shift. This red shift increases slightly as the target angle is increased to 45°. This behavior is interpreted as Brillouin scattering from a flowing plasma with a flow velocity of approximately Mach 1. The 0° − 10° cases show a much broader spectrum with the mean shifted to shorter wavelengths. We tentatively interpret these spectra as being due to scattering from a standing density wave in the plasma. The standing wave arises from four traveling waves, the incident and reflected EM waves plus two ion waves traveling up and down the density gradient of the plasma. This type of interaction is called *modulational instability*[1] scattering.

In Brillouin-like scattering, it is the magnitude of the backscatter fraction which is most important. Figure 14 shows the fraction of

Fig. 15
*Time-resolved backscattered spectra from UV laser-produced plasma.*
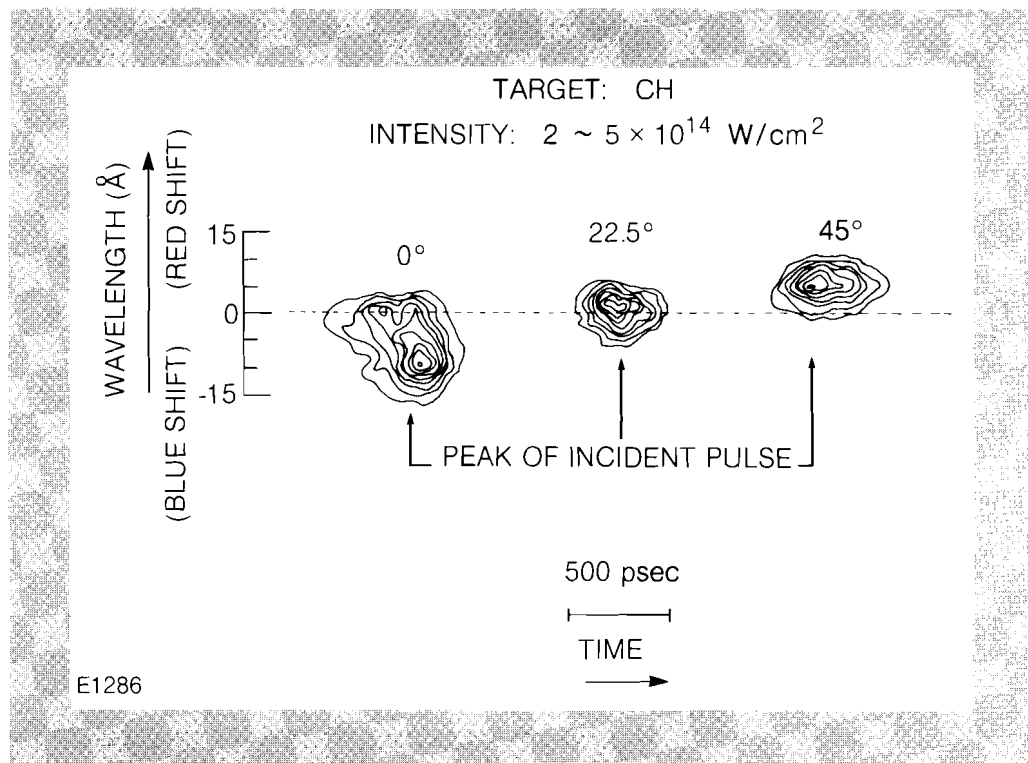
the incident laser energy backscattered by CH targets for 90 and 400 psec pulses. For the 90 psec pulses the backscattering was always less than 2%, suggesting that in these experiments the scale lengths were short enough that the threshold for stimulated scattering was never exceeded. For the 400 psec experiments one notes an increase in backscatter when the average intensity exceeds ~ 10^{14} W/cm². Up to intensities of 10^{15} W/cm the backscatter increases to 5% with no evidence of saturation. It should be noted, however, that the increase is approximately linear with intensity and not exponential.

The Raman and the two plasmon decay processes involve the conversion of the incident EM wave into either one plasma wave and one EM wave (Raman) or two plasma waves ($2\omega_p$ decay). Due to the matching conditions, these processes can only occur at densities less than or equal to quarter critical ($n_c/4$). Both the two plasmon decay and the absolute Raman instabilities can only occur very close to the quarter critical density. (An absolute instability is one which is stationary in space and growing in time.) Another type of Raman instability, the convective Raman instability, occurs at densities below $n_c/4$. This instability involves growing electrostatic plasma waves which move through the plasma.

To observe these effects we have made time integrated, spectrally resolved measurements in the region between 4000 and 7500 Å. Observations were made of light backscattered through the illuminating f/12 lens and at 45° to the incident beam

Fig. 16
Stimulated Raman Backscatter from CH targets for different laser intensities.
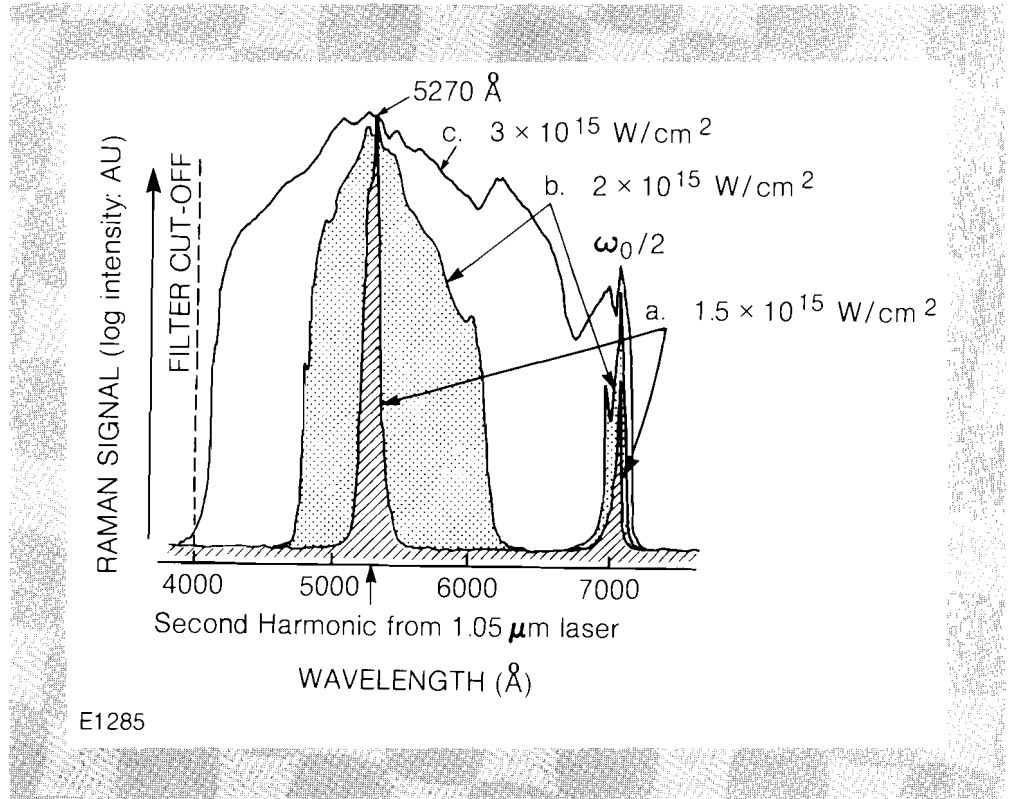
E1285

with an f/3 collecting lens. A typical series of backscatter spectra is shown in Fig. 16. The spectrum shown in curve (a) was taken very close to threshold and shows signals at 7000 Å attributed to the absolute Raman instability and at 5270 Å. The latter arises from convective Raman backscatter driven by a residual green (5270 Å) component present in the incident beam and due to incomplete suppression of the lower harmonics in our UV irradiation facility. Curve (b) was taken at twice the threshold intensity. It shows significant scattering from 4000 to 7000 Å. The two peaks near 7000 Å are again assigned to the absolute Raman instability. The shorter wavelength scattering is attributed to the convective Raman instability. A plot of the Raman intensity versus incident laser intensity is shown in Fig. 17. These curves show very clear threshold behavior for both the absolute instability

Fig. 17

Dependence of Raman instability on incident laser intensity. (a) absolute instability at 7000 Å, (b) convective instability at 6000 Å, (c) convective instability at 5270 Å, (d) energy of Raman scattered light.

E1365
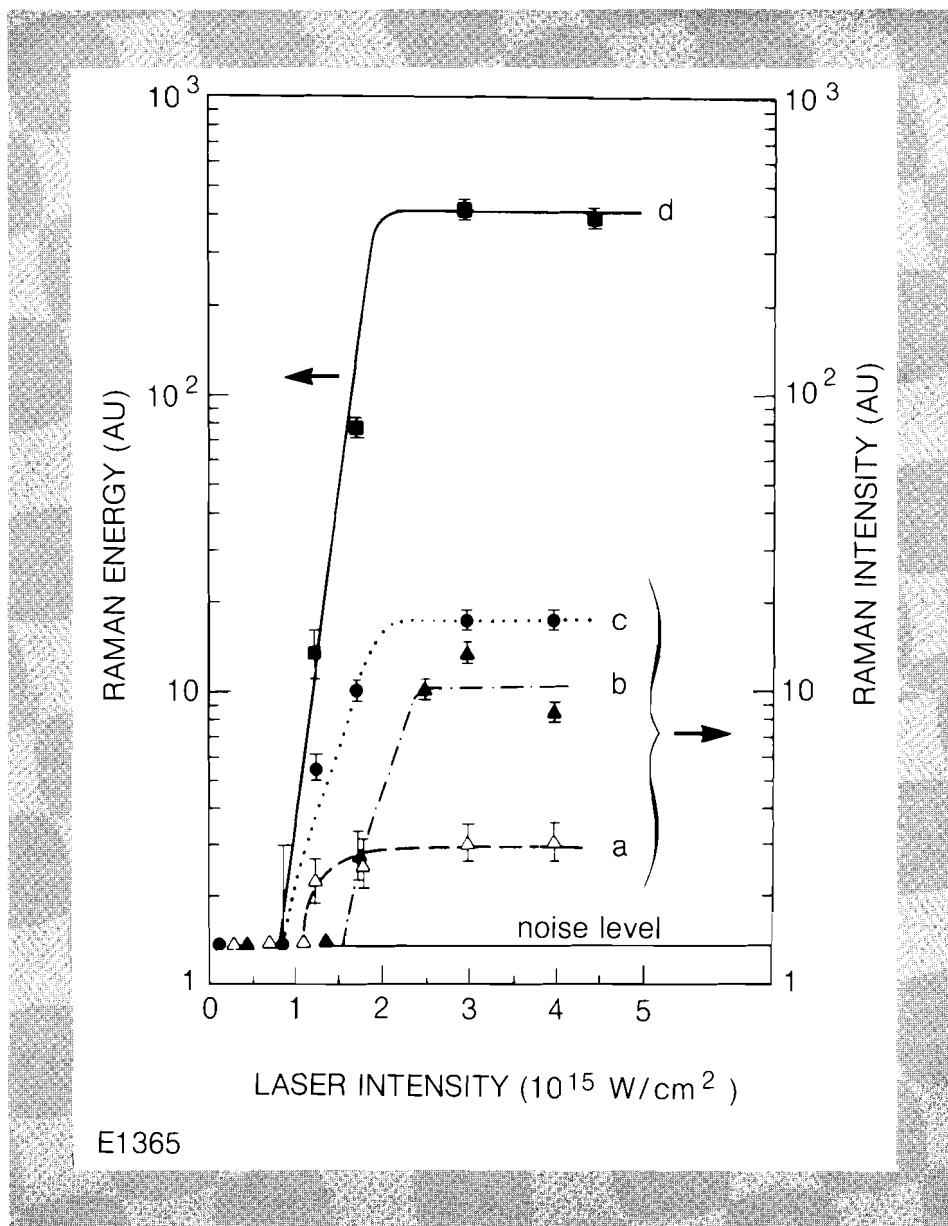
[curve (a)] and the convective instability [curve (b)]. Curve (d) shows the total energy in backscatter in the Raman spectral region and shows an exponential growth followed by a clear saturation. This saturation at very low levels ($\sim 10^{-6}$ of the incident laser energy) is a very encouraging result.

The thresholds for the convective and absolute instabilities are observed to be almost equal. If the effective density scale lengths were the same for both processes the theoretical calculations[2] would predict thresholds which would differ by almost an order of magnitude. From the threshold evidence (Fig. 17), as well as the minimum in the backscattered spectrum at 6600 Å [Fig. 16, curve (b)], we conclude that there must be a steepening of the density profile at quarter critical. This has been predicted in simulations[3] where the steepening was shown to be caused by the two plasmon decay instability.

We do not believe the direct backscatter light at 7000 Å to be due to reconversion of plasma waves back into EM waves because the scattering was found to be highly polarized and we sampled the backscattering only over a very small angle (f/12 cone). In contrast, measurements made at 45° on targets oriented at 45° with respect to the laser beam showed a much lower degree of polarization for the 7000 Å light. However, the same high degree of polarization was found for the shorter wavelength scattering. The difference is attributed to the use of a larger aperture lens (f/3) at 45° compared to the f/12 for direct back-scattering. Since reconversion of the plasmons into EM waves is the inverse of resonance absorption, one expects a minimum in reconversion normal to the target. Experiments to elucidate the difference between absolute Raman and two plasmon decay instabilities are continuing.

These experiments clearly show that both absolute and convective Raman scattering occur for plasmas produced by 400 psec, 0.35 μm light interactions. Fortunately for laser fusion, these instabilities appear to be saturated at rather low levels. The saturation mechanisms are still not well understood.

REFERENCES

1. R. Bingham and C. N. Lashmore-Davies, *Nuclear Fusion* **16**, 67 (1976).
2. C S. Liu, *Advances in Plasma Physics,* edited by A. Simon and W. B. Thompson, vol. **6**, p. 121, (Wiley, N.Y. 1976).
3. A. B. Langdon, B. F. Lasinski, W. L. Kruer, *Phys. Rev. Lett.* **43**, 133 (1979).

2.C Studies of Thermal Electron Transport Inhibition in Steep Temperature Gradients

Thermal conduction of energy by electrons plays a dominant role in the behavior of ablatively accelerated laser fusion targets. It is a consequence of momentum conservation that the energy transported to the ablation surface, by the electrons heated at the critical surface, results in the inward accelerations of the target. Understanding the mechanisms of the thermal conduction process is an essential ingredient in a proper description of the ablative acceleration process required to achieve efficient successful laser-driven implosions of thermonuclear targets.

The commonly used description of thermal conduction was derived by Spitzer and Harm assuming that the electron-ion collision mean-free-path is much smaller than typical temperature scale lengths. In plasmas produced by high-power lasers this assumption fails because of the short scale lengths and high temperatures encountered near the heat front, yielding in some cases calculated characteristic speeds for the thermal heat flow larger than the local electron thermal speed. To avoid non-physical behavior, the upper limit of the heat flux is often assumed to be the "free streaming" limit for an isotropic Maxwellian distribution, commonly written as $Q_f = \alpha \, n_e k T_e \, (kT_e/m_e)^{1/2}$ where $\alpha = 3 \sqrt{3}/8 \sim 0.65$. However, the analysis of many experimental results, including both long[2,3] and short[4,5,6,7,8] wavelength lasers, suggest that α is smaller by about an order of magnitude; typically $0.03 \leq \alpha \leq 0.1$. The use of such a small value of α, without a physical basis, is unsatisfactory, and has led to large uncertainties in target design and the simulation of experiments.[9]

The small value of α has been attributed to a variety of anomalous processes, including magnetic fields, ion acoustic instabilities,[10] and electric fields generated by suprathermal electrons,[11] but the importance of the above processes has not yet been demonstrated. In his recent review of ion acoustic turbulence models, Mead[12] has shown that the fluctuation levels required to reduce the flux limiter to the small values needed to model experiments are much too large to be plausible. An alternative explanation for the inhibition of thermal electron transport has been that the Spitzer-Harm (S-H) description should not be applied to steep temperature gradients, and that a correct treatment of classical conduction based on classical Coulomb collisions would result in lower values for the thermal conductivity than previously suggested. Recent numerical solutions[13,14] to the full Fokker-Planck equation indicate a reduction of the thermal heat flux in steep temperature gradients by roughly an order of magnitude from that given by the S-H description. The incorporation of a Fokker-Planck treatment for thermal electron transport in laser fusion simulation codes would be prohibitive, and therefore an approximate treatment, such as will be discussed in this work, is desirable.

The failure of the S-H theory to predict the heat flow in steep temperature gradients arises primarily for the following two reasons:

a. The particle flux in the S-H formalism is not bounded by the upper limit required by the transport equation, resulting in unphysically large particle and heat fluxes in the case of steep gradients.

b. Non-local effects, where long mean-free-path electrons deposit their energy ahead of the thermal region, cause modifications to the temperature profile, including some preheating.

In Subsection I we shall discuss the first effect, which is local in nature, and present a simple extension to the S-H theory by imposing a physically motivated limit on the anisotropic portion of the electron distribution function, resulting in a description of the electron thermal conduction in steep temperature gradients.[15] This model accounts for most (but not all) of the reduction in the heat flux inferred from experiments, and in typical cases gives results approximately equivalent to a flux-limiter of $\alpha \simeq 0.08$. This model is extended in Subsection II to take into account the non-local effects, and as a result the effective flux limiter is reduced somewhat further, to $\alpha = 0.03$-0.05, in agreement with the value needed to explain transport and absorption experiments.

I. Local Model for Transport Limitation

We follow the derivation of the electron thermal conductivity given by Spitzer and Harm. In the presence of small gradients we assume that the distribution function $f(x,v,\mu,t)$ has a weak angular dependence and can be expressed by a diffusion description:

$$f(x,v,\mu,t) = f_o(x,v,t) + \mu f_1(x,v,t), \qquad (1)$$

where f_o and f_1 represent the local isotropic and anisotropic components, respectively. (In more general transport descriptions f_o and f_1 are the first two angular moments of the distribution function.) In Eq. (1), x is the spatial coordinate, v the velocity, and μ the cosine of the angle θ between the velocity vector and the x-direction. In the case of thermal equilibrium f_o is the local Maxwellian, and f_1 can be obtained by taking the first angular moment of the Boltzmann transport equation for f. We assume steady state and charge neutrality, which is equivalent to the zero current condition given by

$$J = (4\pi e/3)\int_o^\infty v^3 \, f_1 \, dv = 0 \quad , \qquad (2)$$

yielding an expression for the self-consistent electric field. We assume Coulomb scattering: the collisional mean-free-path is then $\lambda(v) = \lambda_0 (v/v_{th})^4$, where v_{th} is the thermal velocity $(2kT/m)^{1/2}$, and λ_0 is the total mean-free-path for 90° scattering by multiple collisions at kT $(\lambda_0 = (kT)^2/(\pi n_e(Z+1)e^4 \ln \Lambda))$.[1] Using these assumptions one finds the ratio f_1/f_0 is:

$$\frac{f_1}{f_0} = \frac{\lambda_0}{L} \left(\frac{v}{v_{th}}\right)^4 \left[\left(\frac{v}{v_{th}}\right)^2 - 4.0\right]$$ (3)

where L is defined by $L \equiv (T/|\ dT/dx|\ )$. Finally, the net heat flux Q is defined by $Q = (4\pi m/6)\int_0^\infty v^5 f_1 dv \equiv \int_0^\infty Q(v)dv$, which upon substitution of Eq. (3), yields Fourier's law for heat conduction: $Q = -\kappa dT/dx$, where κ is the S-H electron thermal conductivity for high Z plasmas.

From Eq. (3) it can be seen that f_1/f_0 increases with λ_0/L, and at some velocity, depending on λ_0/L, it becomes greater than unity. However, the S-H diffusion description cannot be valid for $f_1 > f_0$. When f_1 exceeds f_0 the S-H formulation breaks down because the distribution function, f, becomes negative for some μ.[16] Furthermore, for any transport description the particle flux, $v\int d\mu$ $\mu f(\mu) \equiv f_1 v/3$, cannot exceed the free-streaming value $\mu_{max} f_0 v$, where μ_{max} is the maximum allowed average of μ over the distribution function. For a half-isotropic distribution streaming into a vacuum this limit is 0.25 $f_0 v$, resulting in $f_1 \leq 0.75\ f_0$. (For the exteme case of a collimated beam of particles, $f_1 = 3f_0$.) Therefore, at those velocities for which f_1 exceeds f_0, the S-H heat flux, Q(v), becomes unphysically large,[16] independent of the assumed transport treatment.

In the present work no attempt has been made to solve the transport equation in order to obtain the actual $f_1(v)$. However, a simple extension of the S-H local description in steep temperature gradients (high λ_0/L) can be obtained by limiting $f_1(v)$ to an upper limit $f_{1,m}(v)$, before calculating the net heat flux, $Q = \int Q(v)dv$. Choosing $f_{1,m}(v)$, to be the local Maxwellian $f_0(v)$ will result in an upper limit to the S-H local heat flux.

By applying this limitation procedure before performing the integration we use the diffusion value for f_1 at all velocities at which it is applicable ($f_1 < f_0$), and use the upper bound $f_{1,m}$ only where it is required. The commonly used "free-streaming" limit is obtained by using the upper bound value for f_1 for the entire velocity range, independent of whether the diffusion result is applicable or not. As will be shown, this procedure needs to be applied only for high velocities (above ~2.2 v_{th} for large λ_0/L), and therefore one obtains a more restrictive upper bound to the heat flux than the "free-streaming" limit.

In order to carry out this limiting procedure self-consistently, we solve for $f_1(v)$ simultaneously with the neutralizing electric field. We note that using a limited f_1, without self-consistently determining the electric field, results in non-zero currents, and for $\lambda_0/L \sim 0.05$, negative net Q's.

The results of the above treatment are compared to the S-H theory in Fig. 18. Spitzer-Harm theory predicts that the bulk of the energy is carried by electrons with velocities between 2 v_{th} and 3.5 v_{th}. In Fig. 18a, $\lambda_0/L = 0.002$, where S-H theory is expected to

Fig. 18
Spitzer-Harm (dashed curves) and self-consistent flux limited (solid curves) particle flux. f_1/f_0, and heat flux, $Q(v)$ (in relative units). for (a) $\lambda_0/L = 0.002$; and (b) $\lambda_0/L = 0.1$. The maximum absolute value of $Q(v)$ illustrated in (a) is 0.02 of the value in (b).
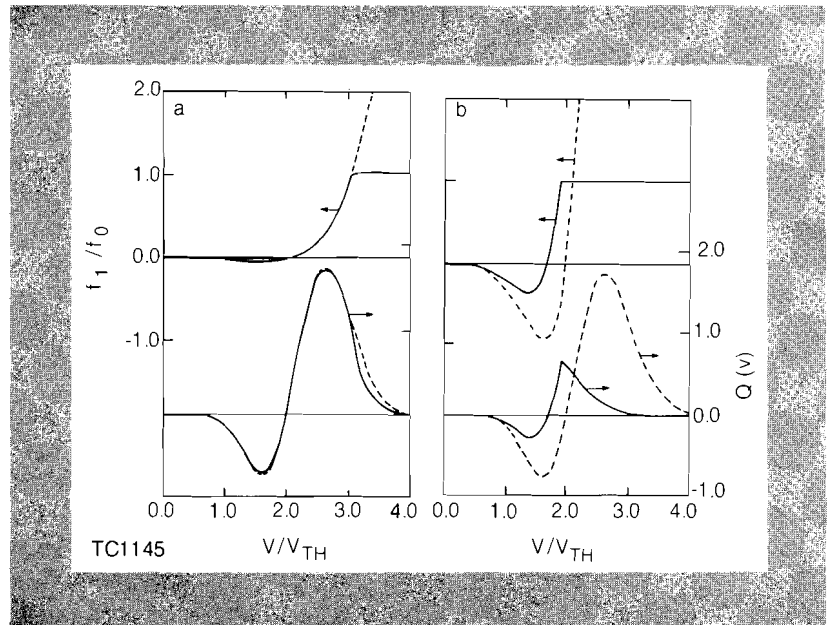
be accurate, f_1 exceeds its maximum value only at $v = 3\ v_{th}$, and since Q is insensitive to $Q(v)$ in this range, the limiting procedure does not significantly change Q from the S-H heat flux for this small λ_0/L. In contrast, note that for $\lambda_0/L = 0.1$ (Fig. 18b), which violates the assumptions of S-H theory as illustrated by f_1 which exceeds f_0 near $v = 2\ v_{th}$, limiting f_1 sharply reduces the heat flux $Q(v)$. Limiting the positive portion of f_1 also results in a substantial reduction in the return current needed to preserve charge neutrality, and hence a reduction in the required electrical field.

The reduction of the heat flux below the S-H value is illustrated in Fig. 19 as a function of λ_0/L. We choose Z = 4 for comparison with Ref. 13 and the e-e contribution to κ is included by using the δ_T of Ref. 1 (for Z =4, $\delta_T \sim 0.5$). The plotted range of λ_0/L extends from 10^{-4}, (where S-H theory applies), to unity, where non-local transport effects dominate. Curve I shows the reduction obtained from the self-consistent treatment when f_1 is limited to its maximum physical value f_0. *This limitation represents a new upper limit to the local S-H heat flux, which is substantially lower than the free-streaming flux (Q_f with $\alpha = 0.65$, curve II).*

To *obtain the correct net heat flux as a function of* λ_0/L the actual dependence of f_1 on v must be obtained. However, to estimate the reduction in the net heat flux a simple model for the transition of f_1 to its maximum value (f_{1m}) was obtained by use of a "harmonic" mean $f_{1\ell} = (f_1^{-1}+f_{1m}^{-1})^{-1}$. Curve III (Fig. 19) shows the results obtained by this method for $f_{1m}=0.75f_0$, which corresponds to a half-isotropic distribution streaming into vacuum $(\mu_{max} = 0.25)$. A choice of f_{1m} between 0.5 f_0 and f_0 is not crucial since Q varies only by 10-25% over this range of f_{1m}. The results of this local treatment (Curve III) yield an order of magnitude reduction in the heat flux, in the range $0.03 < \lambda/L < 0.1$, which is typical of the conditions at the "top of the heat front" where the main thermal inhibition occurs (see Fig. 20 here), and can be seen to agree with
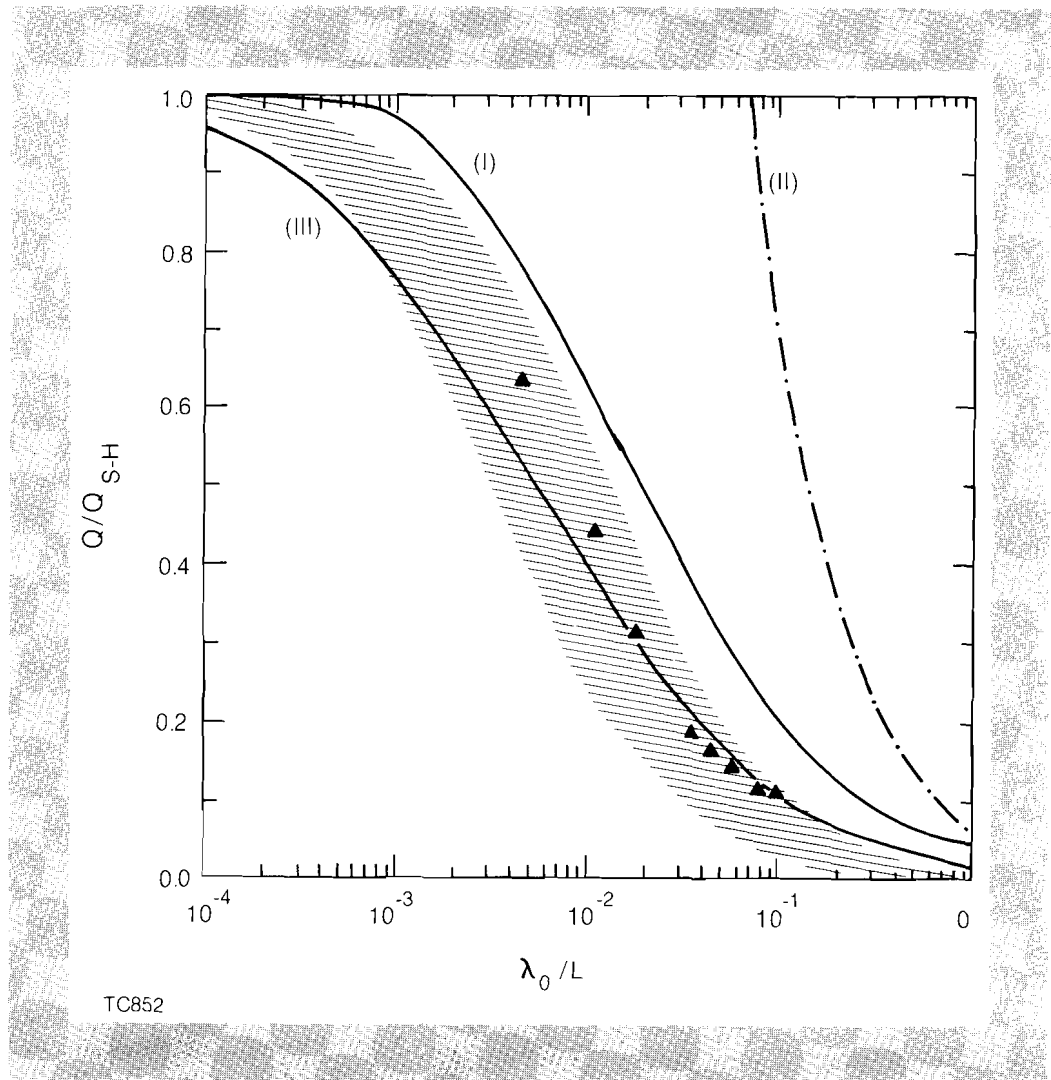
TC852

Fig. 19

Reduction of Spitzer-Harm electron thermal flux as a function of λ_0/L for $Z = 4$:

   I. Self consistent limitation ($f_1 < f_0$) with a sharp cut-off (see Fig. 19);

   II. Free streaming net flux limitation ($\alpha = 0.65$) with a sharp cut-off;

   III. Same as I with $f_1 < 0.75 f_0$ with a "harmonic" cut-off.

The shaded region is bounded by $0.03 < \alpha < 0.1$ using a "harmonic" cut-off. Triangles from Ref. 13: note that the λ_0 of Ref. 13 is a factor of 2.25 higher than that defined here.

the results from Ref. 13. Note that in this region of λ_0/L, the mean free path, λ, of the electrons carrying most of the energy (for $V \sim 2v_{th}$, $\lambda \cong 16\lambda_0$) is approximately equal to the temperature gradient scale length L supporting our premise that the heat flux there is predominantly local. (One might anticipate this result by analogy with the results for the minimum thickness for a strong shock[14].) Our local treatment cannot be applied to predict the preheating at the "base of the front" where nonlocal contributions dominate, due to nearly collisionless electrons streaming from the heated region. The shaded area in Fig. 19 indicates the "inhibition" obtained for $0.03 < \alpha < 0.1$ from using a "harmonic" mean heat flux as in Eqs. (1) and (2), and encompases both Curve III and the results of Ref. 13 (the triangles in the figure). From Fig. 19 we can conclude that the equivalent flux-limiter, α, needed to fit Curve III varies from about 0.05 at $\lambda_0/L \sim 0.01$ to 0.1 at $\lambda_0/L \sim 0.1$, corresponding to respectively lower and higher intensities.

The reduction in the S-H thermal conductivity derived from the new formulation (Curve III in Fig 19) has been introduced into the

hydro-code LILAC. Fig. 20 compares the temperature profile obtained by using the new model with those obtained using the harmonic flux limiter method in the range $0.03 \leq \alpha \leq 0.1$. Both absorption and penetration depth results with the new model are
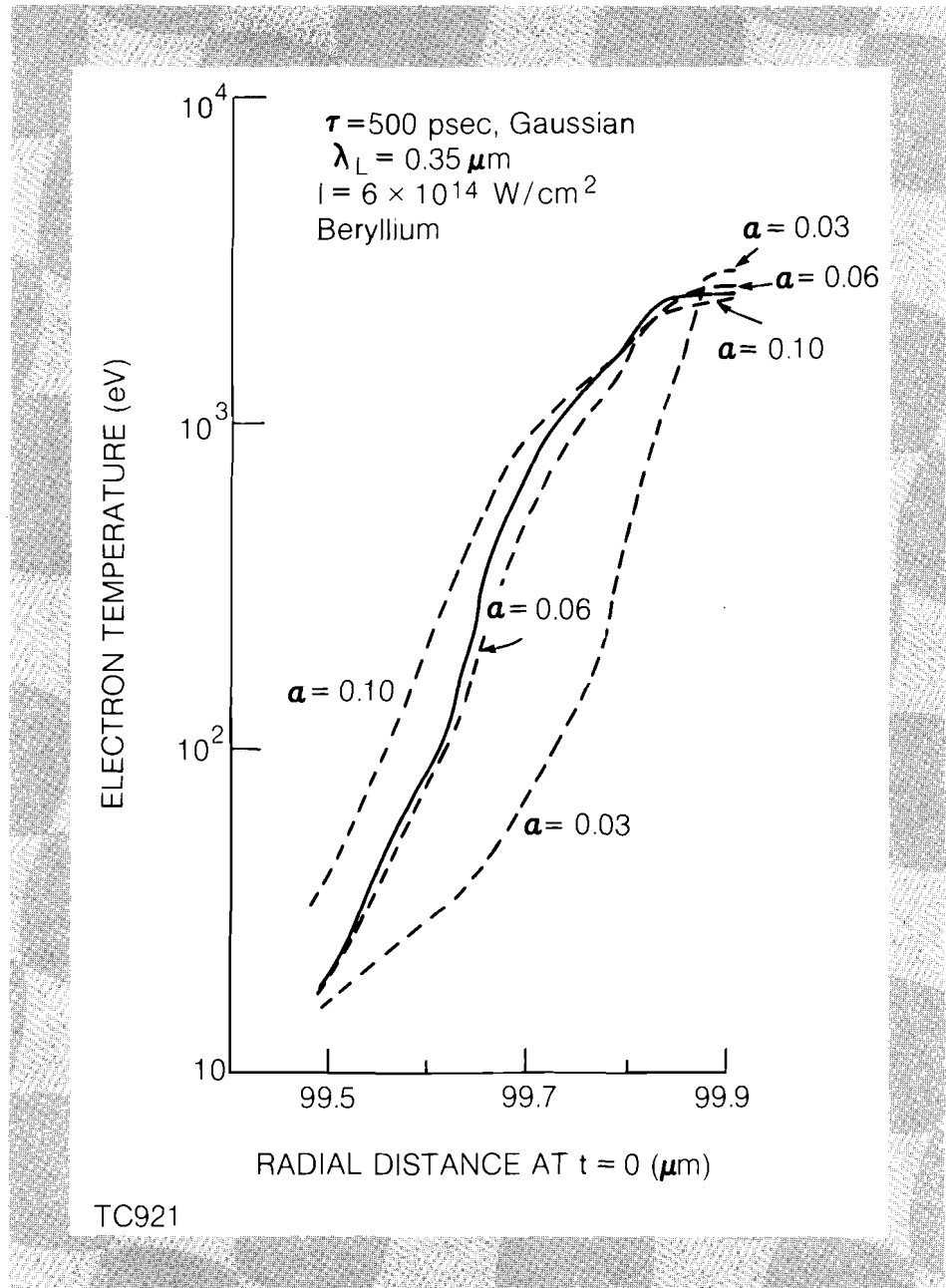

Fig. 20
Temperature profiles in the heat front, plotted at the peak of the pulse against the (initial) Lagrangian coordinate, for the self-consistent local model (solid line) and for the flux-limiter model with various values of f (dashed lines). The target is beryllium, and the laser parameters are: $\lambda_L = 0.35\ \mu m$, $\tau = 500\ psec$, $I = 6\times10^{14}\ W/cm^2$.

similar to those obtained with $\alpha \sim$ 0.06-0.1. Figure 21 shows the temperature profile at the heat front, obtained with the new formulation, along with the ratio λ_0/L. This ratio peaks at the top of the heat front with a value 0.04, thus confirming the assumption that $\lambda_0/L < 0.1$ at the heat front. The general structure of the heat front illustrated Figs. 20 and 21 is typical of a wide range of laser irradiance conditions and target compositions.
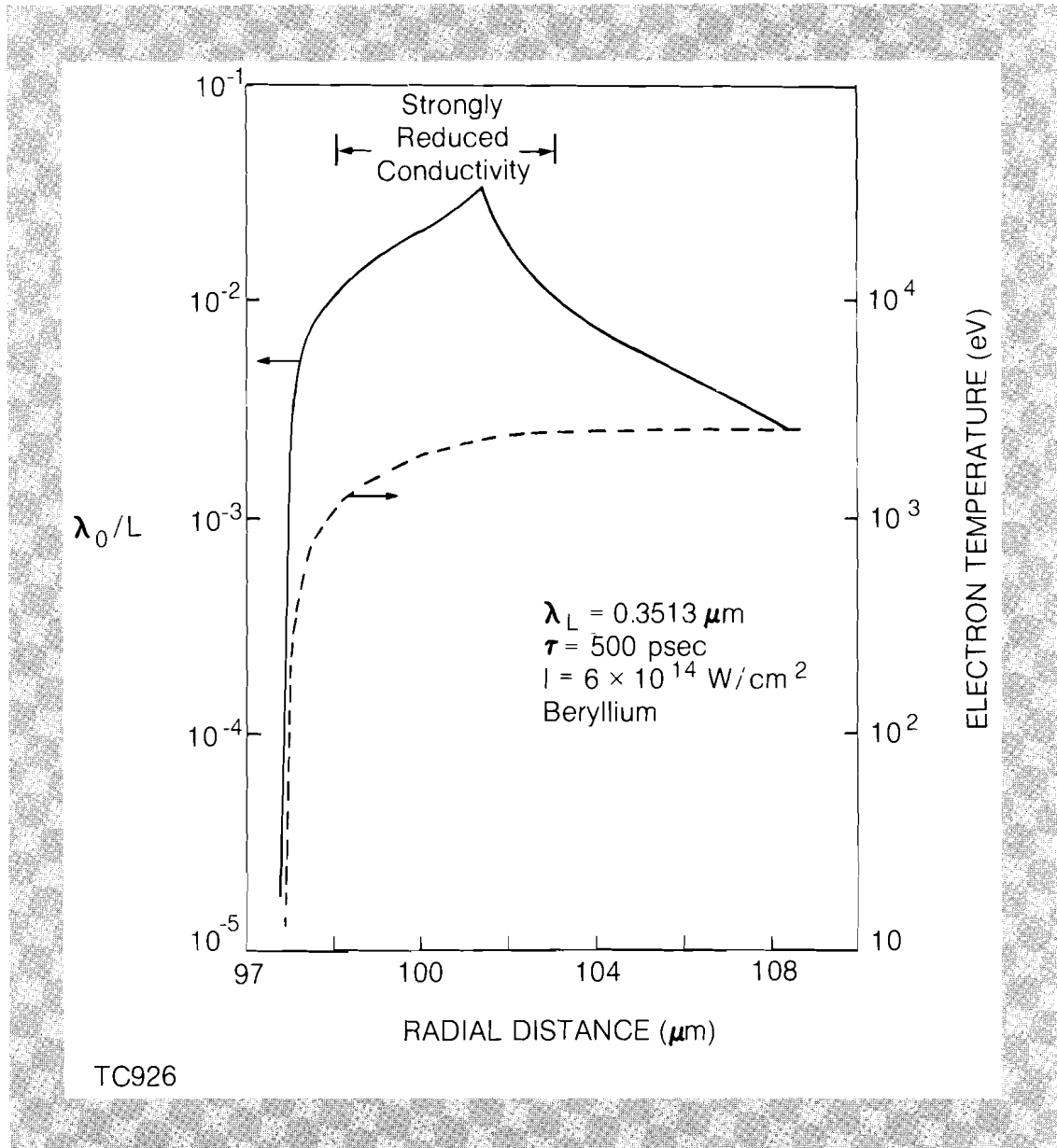
Fig. 21
*Profiles of λ₀/L (solid line) and electron
temperature (dashed line) calculated
by LILAC for the conditions of Fig. 20.*

Figure 22 compares the maximum value of λ_0/L obtained at various irradiation intensities from LILAC simulations using the self consistent formulation with those using a flux limiter of 0.03 and 0.06. The curve for $a = 0.03$ is very close to the corresponding curve in Fig. 5 calculated by SAGE. It is seen that the values of λ_0/L obtained using the self-consistent local model are slightly below those obtained with $\alpha \sim 0.06$ and far below those obtained using $\alpha \sim 0.03$. This result is consistent with the observation made from Figs. 15 and 16 above that the effective flux-limiter ranges from 0.06-0.1 depending on the laser intensity.
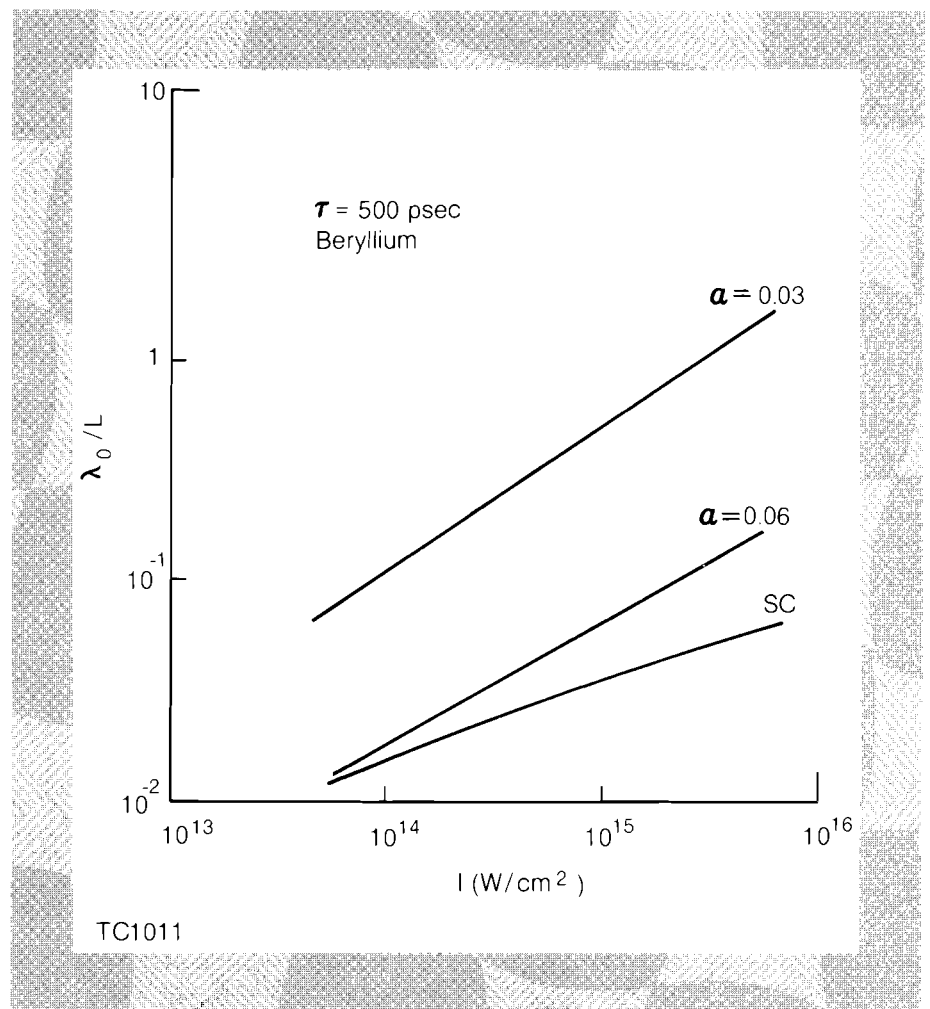
Fig. 22
Dependence of the maximum λ_0/L on laser intensity, for the self-consistent local model and for the flux-limiter model.

## II. Hybrid Model for Non-Local Thermal Transport

We expect the model described above to be applicable for gradients of $\lambda_0/L < 0.1$, where the transport is mainly local in nature. This should be the case in steady heat flow situations, where energy is supplied at the edge of a plasma, and a thermal front propagates into the plasma with its temperature profile adjusting to give $\lambda_0/L < 0.1$. Thus, it is not surprising that the results of our local model and the Fokker-Planck treatment of Ref. 13 are in close agreement.

However, in typical laser-plasma interaction experiments, the laser energy is deposited predominantly in the leading edge of the heat front, causing the temperature gradient there to steepen and give values of λ_0/L in excess of 0.1. Significant non-local energy transport and deposition then takes place, due to the nearly collisionless electrons, resulting in a broadening of the temperature profile at the base of the front and also some preheating. The amount of energy deposited within the characteristic gradient length of the front is reduced, implying a further reduction in the main thermal bulk penetration depth.

In order to account for these non-local contributions, a hybrid model was developed. Here the electrons are treated as a single fluid, except that the energy transport is performed by a multi-group flux-limited diffusion treatment[18] for electrons above some velocity v^*. This velocity is chosen to be the velocity at which the integrated heat flux $(_0\int^{v^*} Q(v)dv)$ is zero, based on the self-consistent local treatment. For the entire range of λ_0/L this v^* lies in the range 2-2.5 v_{th}. From the self-consistent local treatment at velocities up to v^*, $f_1 < f_0$, confirming the assumed local treatment there, and explaining the lack of sensitivity of v^* to the exact form of f_1/f_0 in the flux limited region.

We have compared the hybrid model with a full Fokker-Planck calculation,[19] using a test case similar to that of Ref. 19 where the plasma is heated at one end to a constant temperature. The initial temperature and density profiles are shown in Fig 23 (dotted lines). The temperature in the underdense region ($n_e \cong 10^{21}$ cm^{-3} in this example) is maintained at 1.1 keV throughout. Results are shown for the temperature profiles after 150 psec, as calculated by the hybrid model (dashed line) and the flux-limiter model (solid lines) for $\alpha = 0.05$-0.2. The hybrid result is well approximated by the result for $\alpha = 0.1$, in agreement with the conclusion of Refs. 13 and 19. In this case the contributions of the electrons transported non-locally by the multigroup treatment were relatively small, as expected.

Fig. 23
Initial temperature and density profiles for a transport test problem (dotted lines), and the resulting temperature profiles after 150 psec calculated by the hybrid model (dashed line) and the flux-limiter model (solid lines). The spatial coordinate is Lagrangian.

TC1061   RELATIVE INITIAL DISTANCE (μm)
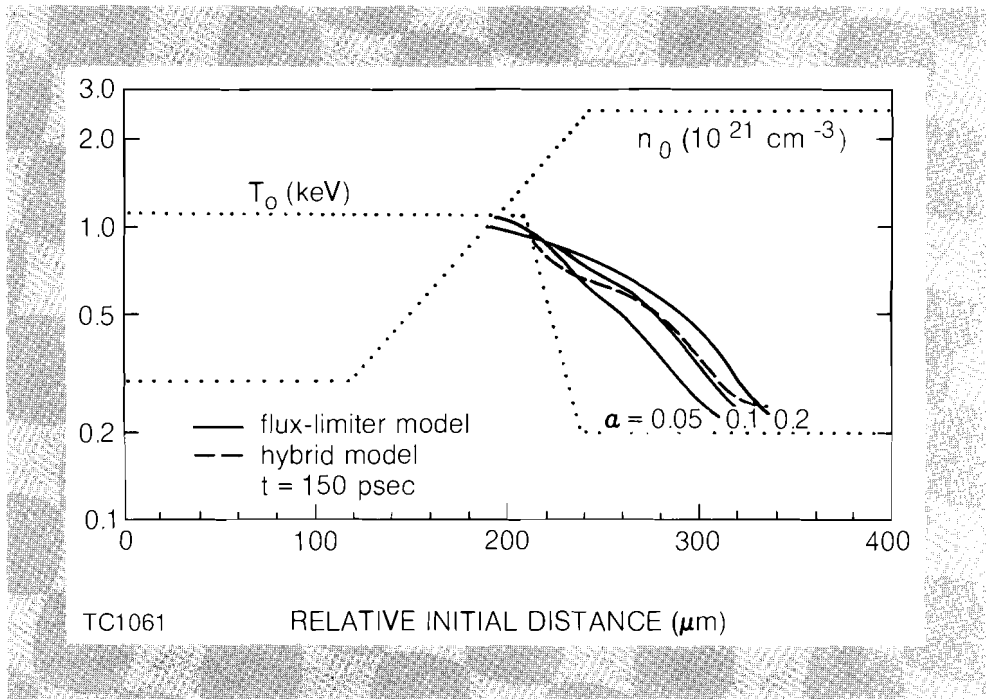
The non-local contributions should however be important under the more general conditions of laser-target interactions. Calculations of absorption and transport, under conditions typical of the 0.35 μm experiments carried out recently at LLE[7,8] (for 400-500 psec pulse widths), are shown in Fig. 24, for the hybrid model and for the flux-limiter model with $\alpha = 0.03$ and 0.06.

- $\lambda = 0.3513\ \mu m,\quad \tau = 500$ psec
- IB absorption only
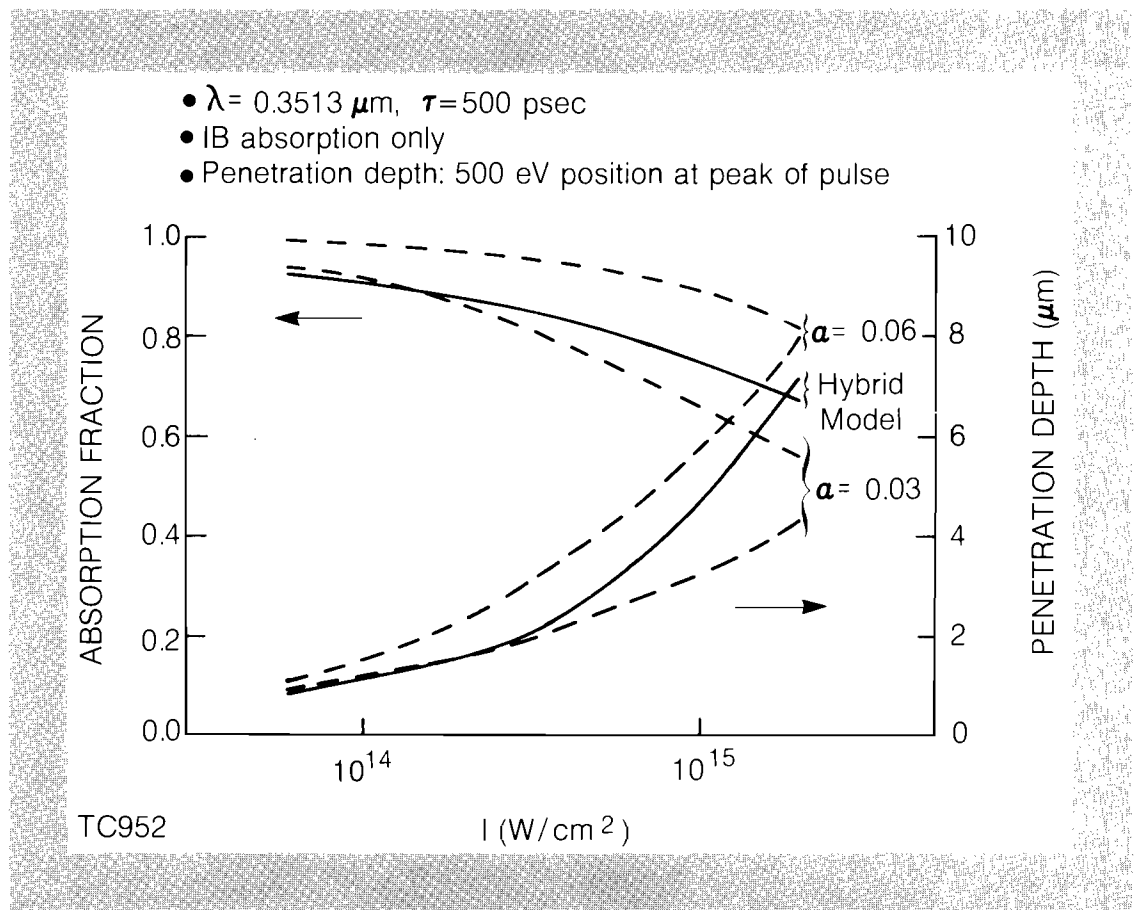- Penetration depth: 500 eV position at peak of pulse

TC952

Fig. 24
Calculated absorption fraction and penetration depth as a function of laser intensity, for the non-local hybrid model (solid lines) and for the flux-limiter model (dashed lines). Targets are CH, and the laser parameters are $\lambda_L = 0.35\ \mu m$ and $\tau = 500$ psec.

No fast electron dump was included in any of these simulations. It is notable that the predictions of the hybrid model, like the experimental results[7,8,] lie within the flux-limiter model predictions for $\alpha = 0.03\text{-}0.06$; in both cases the agreement is best for a value of α closer to 0.03.

In Fig. 25 the temperature profiles are given for typical irradiation conditions, and for the hybrid model and the same two values of α; the horizontal coordinate is a Lagrangian coordinate relative to the initial target position. The steep temperature gradient at the top of the heat front predicted by the hybrid model, and the smoothing of the temperature profile at the base of the front as discussed above, are clearly seen. The penetration depth, defined here by the excursion of the 500 eV contour at the peak of the pulse, lies between the $\alpha = 0.03$ and $\alpha = 0.06$ predictions in accordance with Fig. 24.

From Fig. 25 it is seen that the corona temperature predicted by the hybrid model is smaller than the result for $\alpha = 0.03$. This occurs because the fastest electrons are not inhibited from streaming out of the corona and into the denser cold material.

Our analysis of heat transport suggests that a distinction should be made between the reduced energy flow across the top of the heat front, which results primarily from the limitation
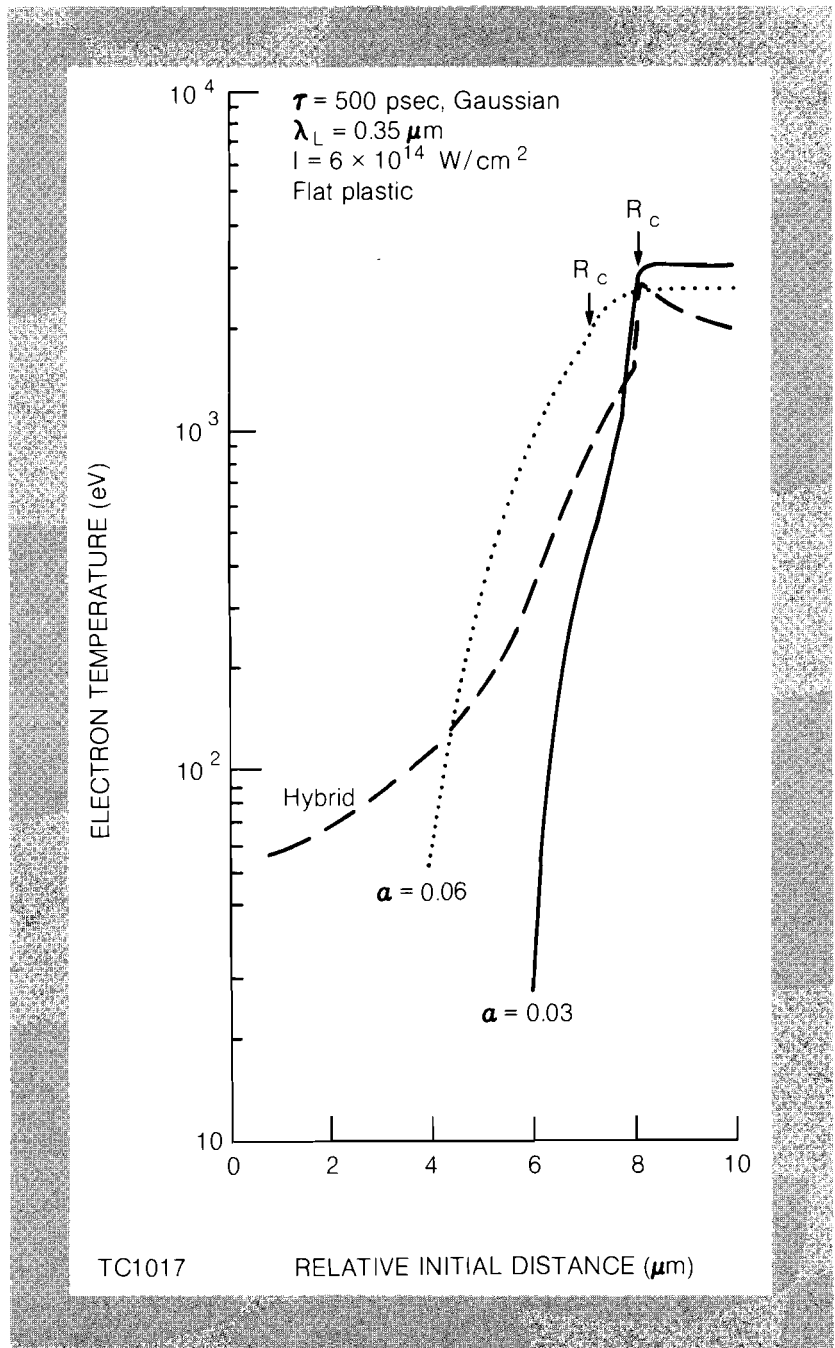
29

Fig. 25
Temperature profiles in the heat front,
plotted at the peak of the pulse against
the (initial) Lagrangian coordinate, for
the hybrid model (dashed line) and the
flux-limiter model with α = 0.03 and
0.06.

imposed on the perturbed distribution function, and the propagation of temperature contours (such as the 500 eV contour used here to identify the "penetration depth"), which depend on the deposition profile of this energy flow. The first process is typically described by a flux-limiter $\alpha \sim 0.08$ (see subsection I). The second effect can be estimated by calculating the fraction of energy deposited within one gradient scalelength L. We assume that this energy causes the heat front to advance, while energy deposited at distances further than L results mainly in preheating. Using simple analytic formulas of energy deposition,[23] we have calculated that less than 50% of the energy flowing across

the top of the heat front is deposited within a distance L, for $\lambda_0/L >$ 0.1. Combining both effects, we obtain an effective flux-limiter of about 0.04 for the propagation of temperature contours.

In summary, we have shown that the 'thermal inhibition" seen in steep temperature gradients, previously attributed to a variety of "anomalous processes", does not require such processes for its explanation. The need for very small flux limiters arose from the incorrect application of the S-H formula far from its regime of applicability, that is when the electrons responsible for the heat flow have mean free paths comparable or greater than the gradient scale length, and a misinterpretation of the classical free-streaming ($\alpha = 0.65$) flux limiter as representing the maximum heat flux. Accounting appropriately for these effects, we have obtained "effective flux limiters" of about 0.03 in good agreement with what has been required to interpret laser plasma interaction experiments.

REFERENCES

1. L. Spitzer and R. Harm, *Phys. Rev.* **89**, 977 (1953).

2. R. C. Malone, R. L. McCrory, and R. L. Morse, *Phys. Rev. Lett.* **34**, 721 (1975).

3. W. L. Kruer, *Comment Plasma Phys. Controlled Fusion* **5**, 69 (1979).

4. F. Amiranoff, R. Fabbro, E. Fabre, C. Garban, J. Virmont, and M. Weinfeld, *Phys. Rev. Lett.* **43**, 522 (1979).

5. D. C. Slater, G. E. Busch, G. Charatis, R. R. Johnson, F. J. Mayer, R. J. Schroeder, J. D. Simpson, D. Sullivan, J. A. Tarvin, and C. E. Thomas, *Phys. Rev. Lett.* **46**, 1199 (1981).

6. W. C. Mead, E. M. Campbell, K. G. Estabrook, R. E. Turner, W. L. Kruer, P. H. Y. Lee, B. Pruett, V. C. Rupert, K. G. Tirsell, G. L. Stradling, F. Ze, C. E. Max, and M. D. Rosen, *Lawrence Livermore National Laboratory Report* **UCRL-84684** (1981).

7. W. Seka, R. S. Craxton, J. Delettrez, L. M. Goldman, R. Keck, R. L. McCrory, D. Shvarts, J. M. Soures, and R. Boni, submitted for publication.

8. B. Yaakobi, T. Boehly, P. Bourke, Y. Conturie, R. S. Craxton, J. Delettrez, J. M. Forsyth, R. D. Frankel, L. M. Goldman, R. L. McCrory, M. C. Richardson, W. Seka, D. Shvarts and J. M. Soures, to be published in Optics Comm.

9. C. E. Max, C. F. McKee, and W. C. Mead, *Phys. Fluids,* **23**, 1620 (1980).

10. W. M. Manheimer, *Phys. Fluids,* **20**, 265 (1977).

11. I. P. Shkarofsky, *Phys. Rev. Lett.* **42**, 1342 (1979).

12. W. C. Mead, *Lawrence Livermore National Laboratory Report,* **UCRL-85246** (1980).

13. A. R. Bell, R. G. Evans, and D. J. Nicholas, *Phys. Rev. Lett.* **46**, 243 (1981).

14. R. J. Mason, *Bull, Am. Phys. Soc.* **25,** 926 (1980); R. J. Mason, *Los Alamos National Laboratory Report* **LA-UR-81-95** (1981).

15. D. Shvarts, J. Delettrez, R. L. McCrory, and C. P. Verdon, *Phys. Rev. Lett,* **47,** 247 (1981).

16. D. R. Gray and J. D. Kilkenny, *Plasma Phys.* **22,** 81 (1980).

17. Ya. B. Zel'dovich and Yu. P. Raizer, *Physics of Shock Waves and High-Temperature Hydrodynamic Phenomena,* (Academic Press, New York, 1966), vol. **1,** chap. 1, p. 84.

18. D. Shvarts, C. Jablon, I. B. Bernstein, J. Virmont, and P. Mora, *Nuc. Fusion* **19,** 1457 (1979).

19. A. R. Bell, Paper 6-1, *11th Annual Anomalous Absorption Conference, Montreal* (1981).

20. M. D. Rosen, *Lawrence Livermore National Laboratory Annual Report* **URCL-50021-79,** p. 3-6 (1979).

Section 3

DEVELOPMENTS IN MICROFABRICATION

3.A Zone Plate Fabrication Developments

A new microfabrication method has been developed for making micro-Fresnel zone plates used in the coded imaging of x-rays and α-particles from laser fusion experiments. Previous work has concentrated on developing individual 25-40 μm thick zone plates. [1,2] However, since each α-particle image requires a new zone plate wihch is approximately 5 μm thick, the present work has concentrated on producing many zone plates from a single master-pattern, thereby eliminating the delicate and time consuming photolithographic steps previously required for each zone plate.

In the new process zone plates are formed by electroplating gold into epoxy molds. The epoxy molds are made by a series of intermediate steps from a single Mylar master-pattern. The process is divided into two phases; fabrication of the master-pattern, and creation of the epoxy replicas from this pattern. The zone plate microfabrication process has many features similar to those developed here at LLE for microhemispherical shell fabrication. [3]

Figure 26 illustrates the five fabrication steps used in constructing a zone plate master-pattern. The sequence begins with a piece of standard 2 mil Mylar. 200 nm of aluminum is evaporated onto one side of the Mylar, which is then spin coated with 1.5 μm of positive photoresist. The zone plate pattern is delineated photolithographically in the photoresist. The exposed aluminum is removed

- Coat Mylar with 200 nm of Al

- Spin photoresist, expose and develop the zone plate pattern

- Chemically etch exposed Al, and remove photoresist

- Reactively sputter etch Mylar

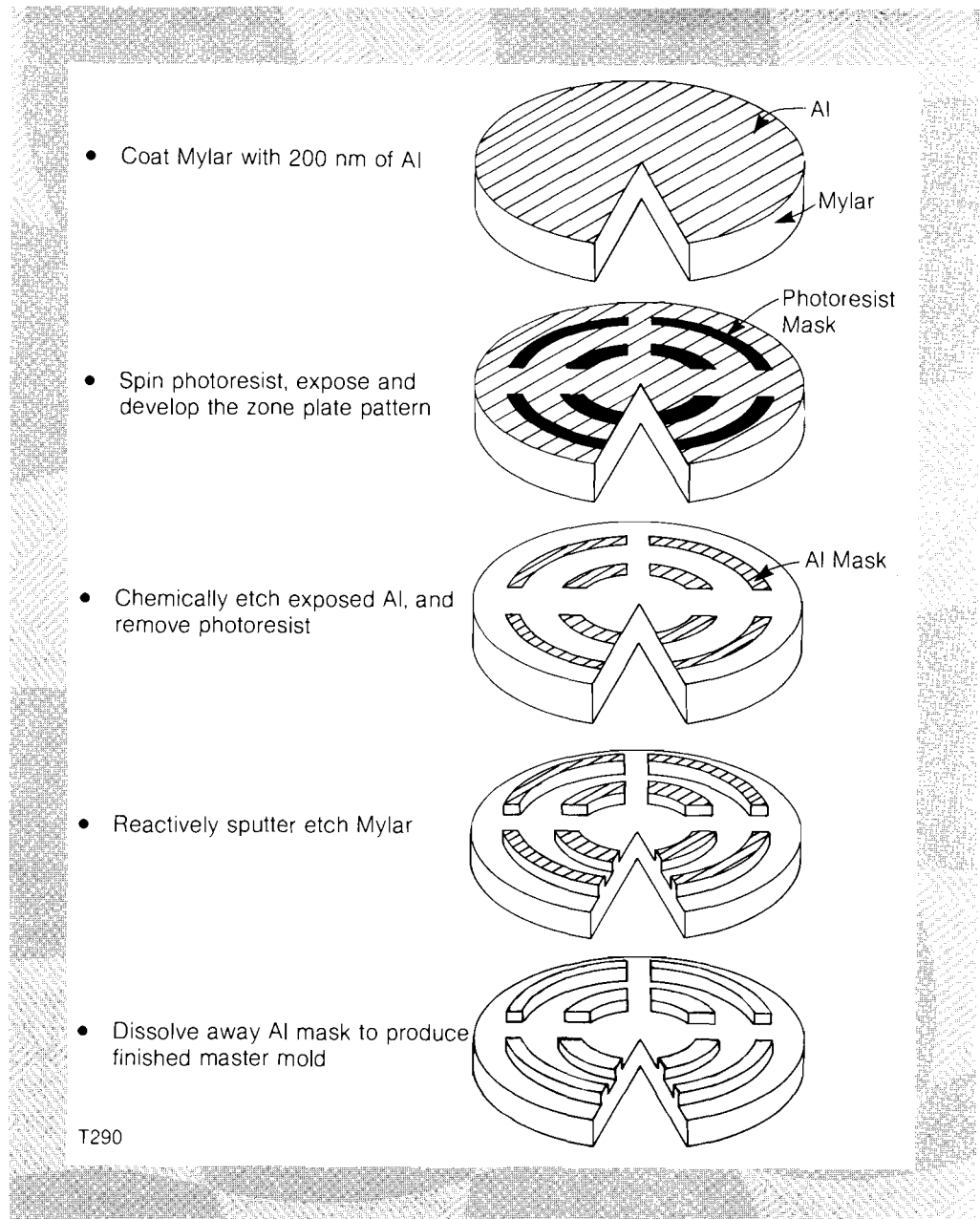- Dissolve away Al mask to produce finished master mold

T290

Fig. 26
The fabrication sequence for master-pattern production. Using photolithography and reactive ion etching a three-dimensional Mylar mold is made.

by chemical etching leaving an integral aluminum mask on th Mylar. This masked Mylar is placed in a reactive sputter etcher[2] and etched with O_2 to a 10 μm depth. The aluminum is finally chemically removed leaving a completed Mylar master-pattern.

Master-pattern replication and final zone plate construction is completed in the five steps illustrated in Fig. 27. Silicone rubber intermediate molds are made by pouring uncured Dow Corning RTV-E onto the Mylar master-pattern at low pressure (200 mT). After curing, the silicone replica mold is separated from the master-pattern and then filled with epoxy, degassed, and pressed onto a planar substrate. Figure 28 is a scanning electron micrograph of an RTV-E intermediate mold and Fig. 29 of an epoxy

cast. Gold is evaporated directionally onto the epoxy cast as a base for plating, as shown in Fig. 27, step 3. Only surfaces normal to the zone plate plane are coated, leaving the tops of the coated cast electrically discontinuous from the bottom which means that no electroplating can occur on the top surfaces. The cast is then electroplated, mounted on a ring, and placed in the reactive sputter etcher to remove the epoxy. This leaves a freestanding 6-10 μm thick gold zone plate. Figure 30 is a scanning electron micrograph of a completed zone plate which has 100 zones and a 5 μm wide outer zone. The diameter of the zone plate is 2 mm.

Fig. 27
Intermediate and final mold production. RTV copies are made of the master-pattern and used to cast the final electroplasting molds in epoxy.

- Cast silicone rubber replicas of master mold

Silicone Rubber

- From replicas cast epoxy final molds

Epoxy Final Mo

- Directionally evaporate Au into final mold

Au

- Electroplate Au

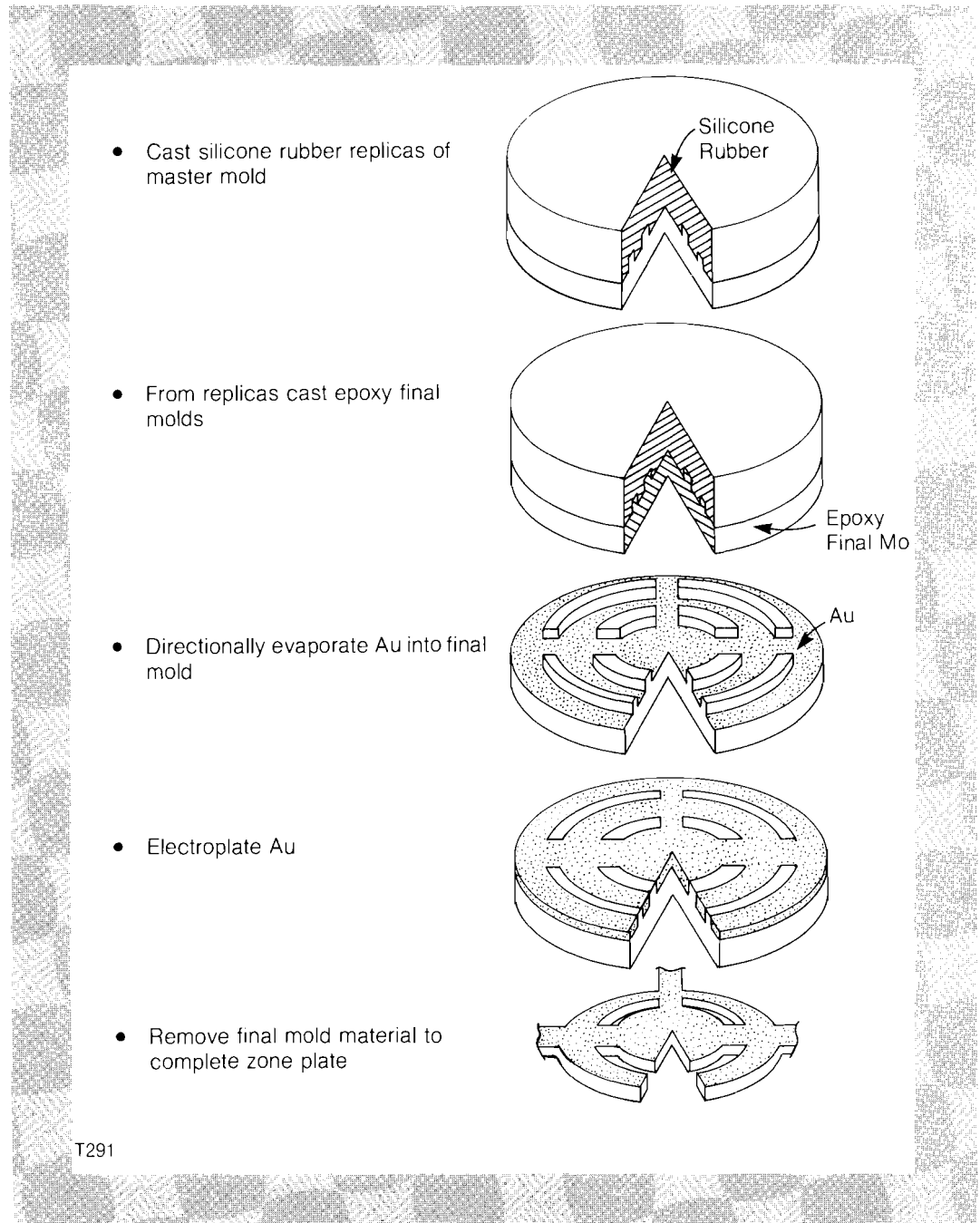- Remove final mold material to complete zone plate

T291

Fig. 28
A scanning electron micrograph of an
intermediate RTV mold made from the
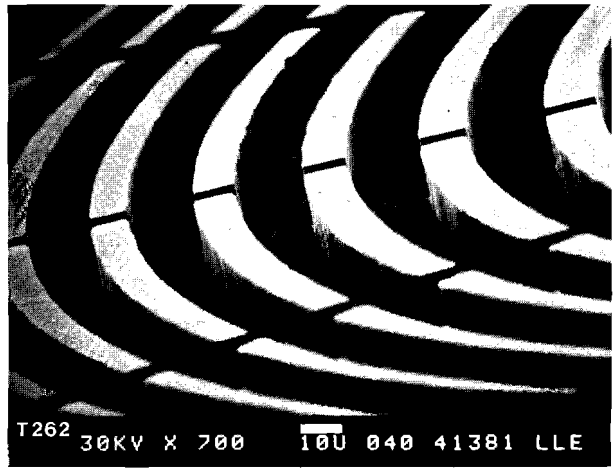Mylar master-pattern.

Fig. 29
A scanning electron micrograph of an
epoxy final mold prior to gold electro-
plating.

This new technique for zone plate fabrication greatly reduces
the number of critically delicate steps, and thus enables fabrication
of 6-10 μm thick zone plates on a production basis. Some
features of the process, such as directionally coating the plating
base onto the final mold, have application to 40 μm thick zone
plate fabrication and other microfabrication techniques.

REFERENCES

1. D. Ciarlo and N. M. Ceglio *Proceedings of SPIE Symposium
    on Semiconductor Microlithography, San Diego,* March,
    1980.

2. F. Kalk and D. Glocker, to be published in *J. Vac. Sci. Tech.*

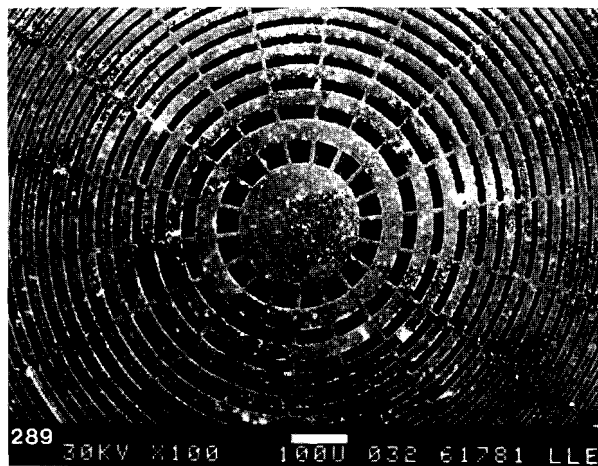3. I. S. Goldstein, F. Kalk and J. Trovato, *J. Vac. Sci. Tech.* 18 (2),
    1981.

Fig. 30
A completed gold zone plate. The
thickness is 5μm, and there are 100
zones with a 5 μm wide outer zone.

3.B Target Pusher Layer Fabrication Developments

The Target Group has recently begun to apply ion beam sputter deposition for target pusher layer fabrication. Metal deposition on both levitated and stalk-mounted fusion targets has been demonstrated. We believe this is the first application of this versatile deposition technique to IF target pusher layer fabrication. Our initial results indicate that ion beam sputtering is far more controllable than the more conventional magnetron sputtering, and its use should permit us to produce better coatings of a wide variety of materials than was previously possible.

In any sputter deposition process, a block of the deposition material (the sputter target) is bombarded by energetic ions, usually of argon. The ions physically eject atoms of the target material, which then deposit on the surrounding surfaces, including the substrate (fusion target core). In conventional plasma sputtering a glow discharge is struck between two electrodes, one of which is constructed from the material to be deposited. A substrate placed in this environment can be rapidly coated by atoms sputtered from the target, producing pusher layers of reasonably high quality. There are, however, several disadvantages to this technique. For example, the substrate is directly exposed to the discharge plasma and as a result is heated by radiation and by energetic electrons from the discharge. This adversely affects the deposited layer's surface quality. In addition, the flux of sputtered atoms, their energy, and the gas pressure all affect the quality of the deposited surface; in a glow discharge, these parameters cannot be independently varied to optimize the deposition process, but rather are coupled through the dynamics of the gas discharge.

Fig. 31
A schematic of an ion beam source. Ions are extracted from the plasma through a grid system and accelerated toward the sputtering target.
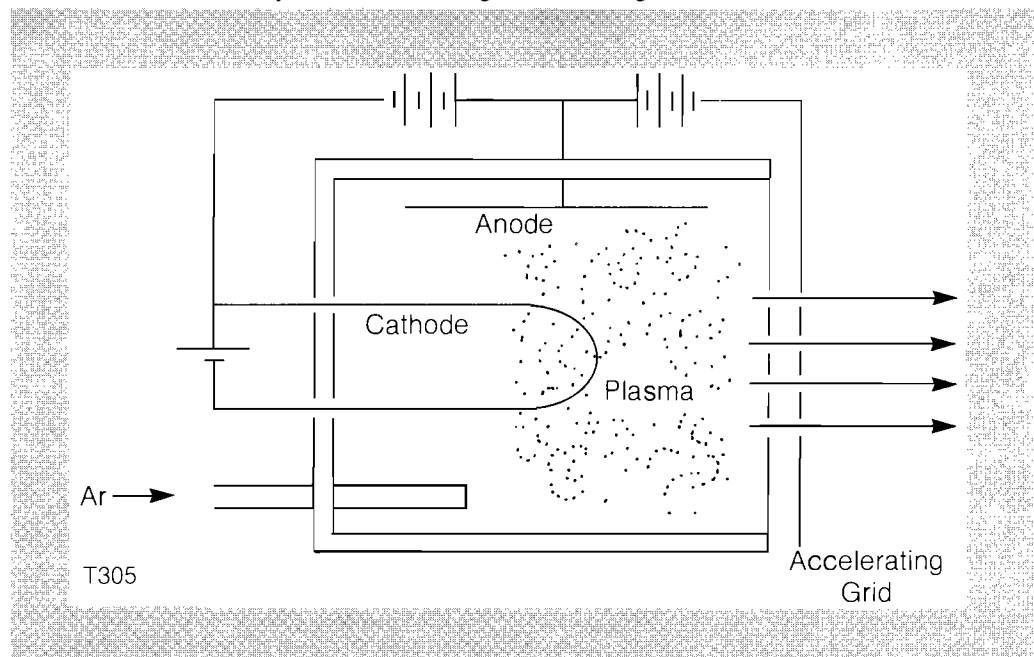
In contrast, ion beam sputter deposition allows much greater control of the deposition process parameters. Figure 31 illustrates an ion beam source. The plasma which produces the ions is confined within a small volume. Ions are extracted from this plasma through a grid and then accelerated through a second grid toward the sputtering target. This permits independent control of the ion flux and the ion energy. Furthermore, the pressure at the location of the sputter target and substrate can be varied over a wide range (~ .005 Pa to .02 Pa) while still maintaining the plasma discharge. Finally, the substrate is not directly exposed to the plasma, thereby reducing the heat load.

The apparatus we have used for the ion beam sputter deposition of pusher layers on stalk mounted microballoons is illustrated in Fig. 32. The sputtering target's conical geometry with the microballoon located in the center of the cone maximizes the deposition rate and improves the deposition uniformity. The microballoon is rotated about an axis perpendicular to the axis of the ion beam and is protected from direct ion beam bombardment by a small masking shield. With this configuration, both copper and iron
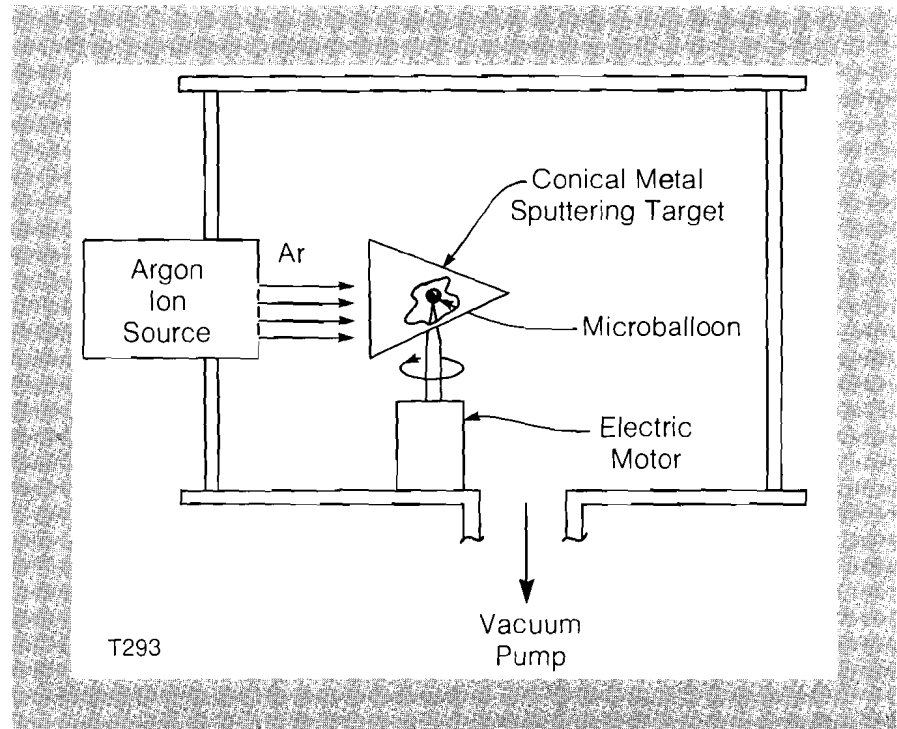

Fig. 32
The apparatus used to ion beam sputter deposit metals onto stalk mounted microballoons. The sputtering target is conical, and the microballoon is rotated in the center of the target.

depositions at rates in excess of 1 μm/hr have been achieved. Pusher layer thickness uniformity, determined by cross sectional measurements of fractured microballoons is typically within 10%. Figure 33 is a scanning electron micrograph of a 1.2 μm thick iron coating produced by ion beam sputter deposition which clearly shows that 1000 Å surface smoothness is achievable.

Figure 34 illustrates the experimental configuration used for ion beam sputter deposition onto levitated target cores. The ions are directed at a planar target which is positioned above the
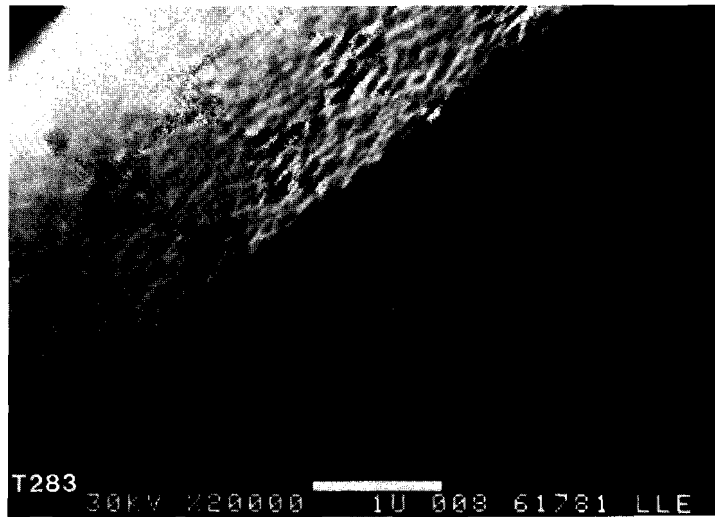
Fig. 33
An iron coating deposited on a stalk mounted microballoon using ion beam sputtering. The thickness is 1.2 µm, and the surface roughness is less than 1000 Å.

levitated balloon. The levitation system consists of a converging array of 25 µm diameter capillaries through which argon gas flows at approximately 1 scc/min[1]. A beveled washer produces an additional radial component to the gas stream flow which provides lateral stability to the levitation. This molecular beam levitation technique has been used with conventional sputtering at LLE,[2] and elsewhere.[3]
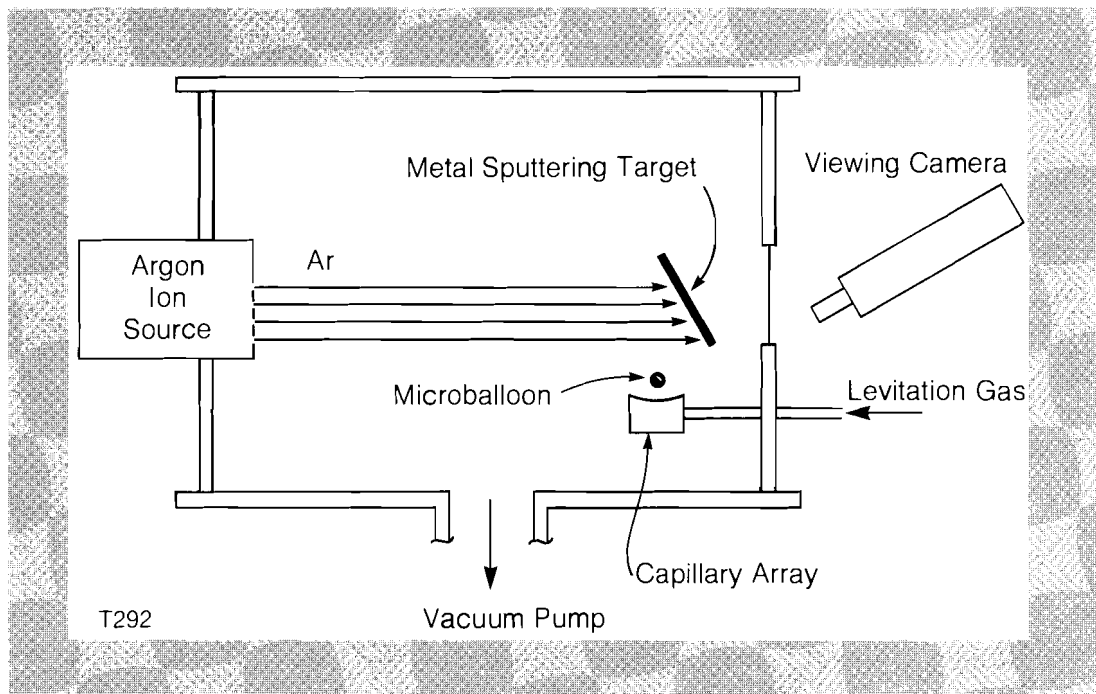

Fig. 34
The apparatus used for ion beam sputter deposition onto levitated microballoons. A focused hole structure produced the Ar molecular beam which was used for levitation.

One serious difficulty usually encountered with glow discharge sputtering onto molecular beam levitated target cores is electrostatic charging due to the proximity of the plasma; the resulting time varying electrostatic force on the balloon makes levitation difficult. We find no evidence of this difficulty for ion beam sputter deposition. However, the low pressures used in ion beam sputtering

reduce damping of the target core's motion which creates other problems. We believe that the target becomes gyroscopically stable about a preferred axis, perhaps due to an undetectable defect in the balloon, and thereafter coats nonuniformly. At some point the target core begins to precess, and soon goes into uncontrollable oscillation. We are studying the possiblility of incorporating magnetic damping to alleviate this problem. Figure 5 is a scanning electron micrograph of a copper surface which has been ion beam sputtered onto a glass microballoon target. Although pusher layer fabrication on levitated target cores is not yet routine, Fig. 35 illustrates that good pusher surface finishes are possible with the ion beam sputter deposition technique.

In summary, the versatility of ion beam sputtering, the availability of a wide variety of sputter target materials, and the encouraging preliminary results demonstrate an important extension of our metal coating capabilities.

REFERENCES

1. J. Varon and I. S. Goldstein, *Rev. Sci. Instr.* **52** 7, (1981).

2. I. S. Goldstein and J. Varon, *J. Vac. Sci. Tech.* **18** 2, (1981).

3. J. K. Crane, *Technical Digest of the Topical Meeting on Inertial Confinement Fusion, San Diego, CA,* 1980.
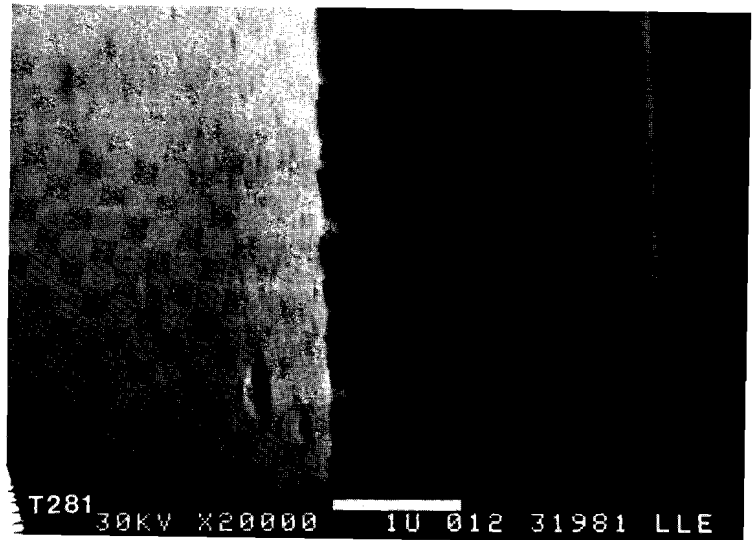

Fig. 35
A copper coating which was deposited on a levitated microballoon using ion beam sputtering. The dense structure and smooth surface of the coating can be seen in this electron micrograph.

Section 4

NATIONAL LASER USERS FACILITY NEWS

This report covers the activities of the National Laser Users Facility (NLUF) during the quarter April to June 1981. During this period the NLUF Steering Committee met to review and rank user proposals. Six of the 21 proposals were accepted for experiments at LLE bringing us to a total of 12 user experiments. We have started user experiments for two groups and during the next quarter will begin a third experiment. Also during this quarter we have continued the planning of implementation of each experiment with out facility and participated in a scienific meeting to acquaint potential users with opportunities for user experiments.

The second NLUF Steering Committee met on April 28 to review and rank proposals, and to recommend funding of approved proposals to the Department of Energy. The committee consisted of scientists from a broad range of areas, including laser fusion, atomic physics, plasma physics, astrophysics, and materials research. The committee membership consists of:

Brian J. Thompson, Chairman, Dean, College of Engineering, University of Rochester.

Thomas C. Bristow, Secretary (non-voting), NLUF Manager

David T. Attwood, Laser Program, Lawrence Livermore National Laboratory

Michael Bass, Center for Laser Studies, University of Southern California

Manfred A. Biondi, Department of Physics, University of Pittsburgh

Donald L. D. Caspar, Rosenstiel Research Center, Brandeis University

Lamar W. Coleman, Laser Program, Lawrence Livermore National Laboratory

Gordon P. Garmire, Department of Astronomy, Pennsylvania State University

Hans R. Griem, Department of Physics, University of Maryland

The committee approved 6 of 21 proposals for user experiments. These experiments are in the areas of phase separation and transition studies of materials using nanosecond x-ray probing; wavelength scaling of the two plasmon decay and stimulated Raman scattering instabilities in laser plasma experiments; a study of the wavelength shifts and spectral broadening of carbon (CVI) Balmer Series Lines; measurements of high resolution spectra in the region of 8 to 780 Å; and a study of opacity effects on line radiation in pellet implosions. These new user experiments are from the following investigators:

1. Mark Sceats (University of Sydney, Australia) – with two experiments.

2. Francis Chen and Chan Joshi (UCLA) and Nizarali Ebrahim (Yale University).

3. Hans R. Griem and J. Adcock (University of Maryland).

4. Uri Feldman and George Doschek (Naval Research Laboratory) and W. E. Behring (Goddard Space Flight Center).

5. C. F. Hooper, Jr. (University of Florida).

These new experiments bring us to a total of 12 users. We are just beginning experiments with the first 6 users and are looking forward to successful experiments with our next group.

We have started experiments with two of our users. Larry Knight and James Thorne from Brigham Young University have started experiments using multi-layer crystals to record the x-ray spectrum from laser produced plasmas. The first part of their experiment was to calibrate these crystals using the Stanford Synchrotron Facility. The next phase has started with target experiments on OMEGA and GDL (the multi-layer crystals are supplied by Troy Barbee of Stanford University). This research is supported by the Department of Energy.

The second user group that has begun experiments is from the University of Rochester. Jim Forsyth and Robert Frankel have been using the x-rays from a laser produced plasma for biological, molecular, and structural kinetic experiments. Successful protein diffraction patterns have been obtained with a new camera system and with 0.35 μm laser radiation. To date, 20-25 joules of

0.35 μm laser have been on target with total x-ray yields of 10^{14} photons per shot (at a wavelength of 4.45Å). Additional details of this research can be found in Volume 3 of the LLE Review (March-May, 1980). This research is supported by the National Science Foundation and the National Institutes of Health. An additional experiment has been x-ray laser development. Repetition of previous experiments with 0.35 μm laser radiation has shown somewhat higher inversion densities than obtained with 1.05 μm radiation.[1] This research is supported by the Air Force Office of Scientific Research.

The NLUF was represented at the Conference on Lasers and Electro-Optics (CLEO) in Washington, DC. An NLUF booth was used to explain the research possibilities and mechanisms for proposal review and acceptance. The presentation attracted a great deal of interest and discussion among visitors to the exhibit. This same format will be used at the American Physical Society Plasma Physics Meeting in New York City from October 13-15.

Further information on the NLUF is available by writing to:

Dr. Thomas C. Bristow
Manager, National Laser Users Facility
Laboratory for Laser Energetics
University of Rochester
250 East River Road
Rochester, NY 14623

REFERENCES

1. V. A. Bhagavatula and B. Yaakobi, *Opt. Comm.* **24**, 331 (1978).

PUBLICATIONS AND CONFERENCE PRESENTATIONS

Publications

T. Sizer, G. Mourou, and R. R. Rice, "Picosecond Dye Laser Pulses Using a CW Frequency Doubled Nd:YAG as the Pumping Source," *Opt. Comm.* **37**, 207-210 (1981).

W. Knox and G. Mourou, "A Simple Jitter-Free Picosecond Streak Camera," *Opt. Comm.* **37**, 203-206 (1981).

B. Yaakobi, S. Skupsky, R. L. McCrory, C. F. Hooper, H. Deckman, P. Bourke, and J. M. Soures, "X-Ray Spectroscopy of Laser Imploded Targets," *Phil. Trans. R. Soc. Lond.* **A 300**, 623-630 (1981).

J. H. Kelly, D. C. Brown, J. A. Abate, and K. Teegarden, "Dynamic Pumping Model for Amplifier Performance Predictions," *Appl. Opt.* **20**, 1595-1605 (1981).

D. C. Brown, J. A. Abate, L. Lund, and J. Waldbillig, "Passively Switched Double-Pass Active Mirror System," *Appl. Opt.* **20**, 1588-1594 (1981).

Forthcoming Publications

W. Knox, W. Friedman, and G. Mourou, "A Simple Silicon Switch-Driven Psec Streak Camera," accepted for publication by *Applied Physics Letters*.

S. Skupsky and S. Kacenjar, "Measuring Fuel ρR for Inertial Fusion Experiments Using Neutron Elastic-Scattering Reactions," accepted for publication by the *Journal of Applied Physics.*

M. True, J. Albritton and E. Williams, "Fast Ion Production by Suprathermal Electrons in Laser Fusion Plasmas," accepted for publication by *Physics of Fluids.*

R. L. McCrory, L. Montierth, R. Morse and C. Verdon, "Taylor Instability in Fusion Targets," to be published in *Laser Interactions and Relative Plasma Phenomena,* vol. V., Plenum Press.

J. Soures, T. Bristow, H. Deckman, J. Delettrez, A. Entenberg, W. Friedman, J. Forsyth, Y. Gazit, G. Halpern, F. Kalk, R. McCrory, D. Peiffer, J. Rizzo, S. Skupsky, E. Thorsos, B. Yaakobi, and T. Yamanaka, "A Review of High Density Laser Driven, Implosion Experiments at the Laboratory for Laser Energetics," to be published in *Laser Interactions and Relative Plasma Phenomena,* vol. V., Plenum Press.

T. Nordland and W. Knox, "Lifetime of Fluorescence from Light-Harvesting Chlorophyll a/b Proteins: Excitation Intensity Dependence," submitted for publication to *Biophysical Journal.*

G. Mourou, "D.C. High Voltage Switching," submitted for publication to *Optics Communication.*

D. Shvarts, J. Delettrez, R. McCrory and C. Verdon, "Self-Consistent Reduction of the Spitzer-Harm Electron Thermal Heat Flux in Steep Temperature Gradients," submitted for publication to *Physical Review Letters.*

S. Kacenjar, L. Goldman and A. Entenberg, "Copper Activation Counter Calibration Using Solid State Track Detectors," accepted for publication by *Review of Scientific Instruments.*

L. Goldman and S. Sarraf, "Effects of Prepulse on Non-Thermal (>10 keV/Z) Ions in Laser Produced Plasma," submitted for publication to *Physical Review A.*

S. Sarraf, E. Williams and L. Goldman, "Ion-Ion Two-Stream Instability in Multispecies Stream Plasma," submitted for publication to *Physical Review Letters.*

R. W. Anderson and W. Knox, "Time-Resolved Fluorescence Decay Measurements in Phthalazine," submitted for publication to the *Journal of Luminescence.*

G. Albrecht and J. Bunkenburg, "Active-Passive Mode-Locked Oscillator Generating Nanosecond Pulses," accepted for publication by *Optics Communications.*

K. Tanaka, L. M. Goldman, W. Seka, M. C. Richardson, and J. M. Soures, "Stimulated Raman Scattering from UV Laser-Produced Plasmas," submitted for publication to *Physical Review Letters.*

B. Yaakobi, T. Boehly, P. Bourke, Y. Conturie, R. S. Craxton, J. Delettrez, J. M. Forsyth, R. D. Frankel, L. M. Goldman, R. L. McCrory, W. Seka, and J. M. Soures, "Characteristics of Target Interaction with High Power UV Laser Radiation," submitted for publication to *Optics Communication.*

G. M. Halpern, "An Improved Method for the Nondestructive Assay of the Tritium Content of Glass Microballoon Laser Fusion Targets," submitted for publication to *Journal of Fusion Energy.*

W. Seka, R. S. Craxton, J. Delettrez, L. M. Goldman, R. Keck, R. L. McCrory, D. Shvarts, J. M. Soures, and R. Boni, "Measurements and Interpretation of the Absorption of 0.35 μm Laser Radiation on Planar Targets," submitted for publication to *Physical Review Letters.*

D. C. Brown, J. H. Kelly and J. A. Abate, "Active Mirror Amplifiers: Progress and Prospects," submitted for publication to the *Journal of Quantum Electronics: Special Issue for Laser Fusion.*

G. Albrecht and G. Mourou, "A Long Pulse/Short Pulse Synchronization Scheme Using a Regenerative Amplifier and High Voltage Semiconductor Switching," submitted for publication to the *Journal of Quantum Electronics: Special Issue for Laser Fusion.*

R. S. Craxton, S. D. Jacobs, J. E. Rizzo, and R. Boni, "Basic Properties of KDP Related to the Frequency Conversion of 1 Micron Laser Radiation," submitted for publication to the *Journal of Quantum Electronics: Special Issue for Laser Fusion.*

R. S. Craxton, "High Efficiency Frequency Tripling Schemes for High Power Nd:Glass Lasers," submitted for publication to the *Journal of Quantum Electronics: Special Issue for Laser Fusion.*

J. Bunkenburg, W. Seka and J. M. Soures, "The OMEGA High Power Phosphate Glass System: Design and Performance," submitted for publication to the *Journal of Quantum Electronics: Special Issue for Laser Fusion.*

J. Boles, D. Pessel and L. Forsley, "OMEGA Automated Laser Control and Data Acquisition," submitted for publication to the *Journal of Quantum Electronics: Special Issue for Laser Fusion.*

W. Seka, J. M. Soures, S. D. Jacobs, L. Lund, R. S. Craxton, "GDL: A High Power 0.35 μm Laser Facility," submitted for publication to the *Journal of Quantum Electronics: Special Issue for Laser Fusion.*

Conference Presentations

K. K. Lee, R. Hopkins, and R. L. McCrory, "Uniformity of Illumination on Spherical Targets for the OMEGA System," presented at the Topical Conference on Symmetry Aspects of Inertial Fusion Implosions, May 1981.

C. P. Verdon, R. L. McCrory, and R. L. Morse, "Nonlinear Development and Effects of Multi-Frequency Hydrodynamic Instabilities in Ablatively Accelerated Thin Shells," presented at the Topical Conference on Symmetry Aspects of Inertial Fusion Implosions, May 1981.

R. Bingham, R. Short, E. Williams, D. Villeneuve and M. C. Richardson, "Filamentation at Short Wavelengths," presented at

the Topical Conference on Symmetry Aspects of Inertial Fusion Implosions, May 1981.

R. L. McCrory, C. P. Verdon, J. Delettrez and D. Shvarts, "Wavelength Scaling and Illumination Uniformity Requirements for Laser Fusion," presented at the Topical Conference on Symmetry Aspects of Inertial Fusion Implosions, May 1981.

R. Bingham, R. Short, E. Williams, D. Villeneuve, and M. C. Richardson, "Filamentation at Short Wavelengths," presented at the Eleventh Annual Conference on Anomalous Absorption of Electromagnetic Waves, June 1981.

C. P. Verdon, R. L. McCrory and R. L. Morse, "Nonlinear Development of Multi-Frequency Rayleigh-Taylor Instability in Ablation Driven Thin Shells," presented at the Eleventh Annual Conference on Anomalous Absorption of Electromagnetic Waves, June 1981.

J. Delettrez, R. L. McCrory, D. Shvarts, C. P. Verdon, and B. Yaakobi, "Analysis of Thermal Electron Transport, 'Inhibition' in Laser Plasma Interactions Under Various Laser and Target Conditions," presented at the Eleventh Annual Conference on Anomalous Absorption of Electromagnetic Waves, June 1981.

R. S. Craxton, J. Delettrez, R. L. McCrory, D. Shvarts, R. Keck, and W. Seka, "Theoretical Interpretation of Short Wavelength Interaction Experiments," presented at the Eleventh Annual Conference on Anomalous Absorption of Electromagnetic Wave, June 1981.

E. A. Williams, R. Short, and R. Bingham, "Propagation Effects on Raman Spectra," presented at the Eleventh Annual Conference on Anomalous Absorption of Electromagnetic Waves, June 1981.

R. W. Short, R. Bingham, and E. A. Williams, "Filamentation of Electromagnetic Radiation in Flowing Plasmas," presented at the Eleventh Annual Conference on Anomalous Absorption of Electromagnetic Waves, June 1981.

D. Shvarts, J. Delettrez, R. L. McCrory, and C. P. Verdon, "A Self-Consistent Flux-Limited Extension of the Spitzer-Harm Thermal Conductivity in Steep-Temperature Gradients," presented at the Eleventh Annual Conference on Anomalous Absorption of Electromagnetic Waves, June 1981.

L. Goldman, K. Tanaka, W. Seka, E. Williams, and R. Bingham, "Time-Resolved Measurements of Brillouin Backscatter from Plasmas Produced by 0.35 μm Laser," presented at the Eleventh Annual Conference on Anomalous Absorption of Electromagnetic Waves, June, 1981.

W. Seka, L. Goldman, M. Richardson, J. Soures, B. Yaakobi, T. Boehly, R. Keck, K. Tanaka, D. M. Villeneuve, R. Boni, R. Bingham, R. S. Craxton, J. Delettrez, R. L. McCrory and E. Williams, "0.35 μm Interaction Experiments at LLE," presented at the Eleventh Annual Conference on Anomalous Absorption of Electromagnetic Waves, June 1981.

B. Yaakobi, T. Boehly, P. Bourke, J. Delettrez, L. M. Goldman, R. L. McCrory, W. Seka, and J. M. Soures, "Heat Transport, Ablation

Rate and Pressure Measurements in UV-Laser Target Interaction Experiments," presented at the Eleventh Annual Conference on Anomalous Absorption of Electromagnetic Waves, June 1981.

J. H. McAdoo and L. M. Goldman, "100 keV X-Ray Continuum from Two-Plasma Decay," presented at the Eleventh Annual Conference on Anomalous Absorption of Electromagnetic Waves, June 1981.

K. Tanaka, L. M. Goldman, M. Richardson and W. Seka, "Spectrally Resolved Measurements of Raman Backscatter from Plasmas Produced by 0.35 μm Laser," presented at the Eleventh Annual Conference on Anomalous Absorption of Electromagnetic Waves, June 1981.

S. D. Jacobs and J. A. Abate, "Compatibility of Transmissive Optical Materials with High Intensity 0.351 μm Laser Radiation," presented at the Annual Meeting of the Conference on Lasers and Electro-Optics, June 1981.

J. A. Abate, "Laser Damage Thresholds of Optical Coatings at 0.351 μm," presented at the Annual Meeting of the Conference on Lasers and Electro-Optics, June 1981.

W. Seka, L. M. Goldman, M. C. Richardson, J. M. Soures, B. Yaakobi, T. Boehly, R. Keck, K. Tanaka, L. Forsley, R. Boni, R. S. Craxton, J. A. Delettrez, and R. L. McCrory, "0.35 μm Laser/Matter Interaction Experiments at the University of Rochester," presented at the Annual Meeting of the Conference on Lasers and Electro-Optics, June 1981.

K. Tanaka, L. Goldman, W. Seka, J. Soures, R. S. Craxton, "Backscatter Measurements in 0.35 μm Irradiation Experiments," presented at the Annual Meeting of the Conference on Lasers and Electro-Optics, June 1981.

B. Yaakobi, P. Bourke, Y. Conturie, L. M. Goldman, W. Seka, J. M. Soures, R. S. Craxton, J. Delettrez, R. L. McCrory, and S. Skupsky, "Heat Transport Measurements in the Irradiation of Flat Targets with a Frequency-Tripled ($\lambda = 0.35$ μm) Nd:Glass Laser," presented at the Annual Meeting of the Conference on Lasers and Electro-Optics, June 1981.

G. Albrecht and G. Mourou, "Regenerative Amplifier Development at the Laboratory for Laser Energetics," presented at the Annual Meeting of the Conference on Lasers and Electro-Optics, June 1981.

R. Sobolewski, C. V. Stancampiano and G. Mourou, "Transient Effects in Superconducting Thin Films Illuminated by a Picosecond-Pulse Laser," presented at the Annual Meeting of the Conference on Lasers and Electro-Optics, June 1981.

W. Knox, G. Mourou, A. Antonetti, G. Hamoniaux, G. Grillon, and R. Astier, "A Stable Single Shot Averaging Picosecond Streak Camera," presented at the Annual Meeting of the Conference on Lasers and Electro-Optics, June 1981.

S. Williamson, S. Letzring, and G. Mourou, "Picosecond Switching with Photoelectrons," presented at the Annual Meeting of the Conference on Lasers and Electro-Optics, June 1981.

R. Keck, W. Seka, L. M. Goldman, J. M. Soures, R. Boni, L. Forsley, R. S. Craxton, J. Delettrez, and R. L. McCrory, "Absorption of 0.35 μm Radiation in Laser/Matter Interaction Experiments," presented at the Annual Meeting of the Conference on Lasers and Electro-Optics, June 1981.

A. E. Rosenbluth and J. M. Forsyth, "Difference Equation Analysis of X-Ray Multilayer Reflectors," presented at the Topical X-Ray Conference, June 1981.